# FINAL TECHNICAL REPORT

## September 1994

DTIC
ELECTE
FEB 1 7 1995
S
G
D
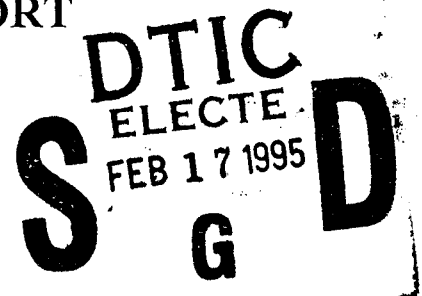
# INNOVATIVE PROCESSING
# OF
# COMPOSITES FOR ULTRA-HIGH
# TEMPERATURE APPLICATIONS

CLEARED
FOR OPEN PUBLICATION

by

JAN 3 1 1995     6

DIRECTORATE FOR FREEDOM OF INFORMATION
AND SECURITY REVIEW (OASD-PA)
DEPARTMENT OF DEFENSE

Reza Abbaschian
Department of Materials Science and Engineering
University of Florida
Gainesville, Florida

94-31948

19950210 055

# BOOK IV of IV

# Executive Summary

The overall objective of this program was to provide a fundamental understanding of the processing science and technology necessary to fabricate ceramic-matrix, intermetallic-matrix, and metal-matrix composites with superior mechanical properties in high temperature and oxidizing environments. The composites are intended for use as structural materials for advanced aerospace applications at temperatures exceeding 1200°C (2200°F).

In order to accomplish the program objective, interactive research groups were established in three key areas of (a) Fiber Fabrication, (b) Coatings and Infiltration, and (c) Composite Fabrication. The objective of the fiber fabrication group was to develop new fibers which have superior strength and toughness at high temperatures and in oxidizing environments. The research effort focused on the development of two types of fibers: (1) glass-free mullite-based fibers, and (2) oxygen-free silicon carbide fibers. The coatings program had two primary objectives: (1) to control the characteristics of matrix/reinforcing phase interfaces (e.g., to control chemical reactions and bonding at a matrix/fiber interface) and (2) to develop coatings that will improve the oxidation resistance of metal-matrix and intermetallic-matrix composites. Coatings methods utilized included chemical vapor deposition, sol-gel processing, and solution coating with polymeric precursors to ceramics.

The composite fabrication group investigated various methods to incorporate reinforcing phases (i.e., fibers, whiskers, and particulates) into ceramic-, metal-, and intermetallic-matrices. Processing methods investigated included colloidal processing, chemical vapor infiltration, reactive hot-compaction and *in situ* coating, and microwave sintering. The objectives were not only to utilize innovative processing techniques, but also to develop and improved scientific understanding of processing-microstructure relationships in composites fabrication.

This annual report consists of seven sections compiled in four books as described below:

**BOOK I**

| | | |
|---|---|---|
| Section 1 | Processing and Properties of Silicon Carbide Fibers | |
| | Principal Investigators: | C.D. Batich |
| | | M.D. Sacks |
| | | |
| Section 2 | Processing of Mullite Composite Fibers | |
| | Principal Investigators: | J.H. Simmons |
| | | M.D. Sacks |
| | | A.B. Brennan |
| | | |
| Section 3 | Chemical Vapor Deposition (CVD) and Chemical Vapor Infiltration (CVI) | |
| | Principal Investigator: | T.J. Anderson |

**BOOK II**

Section 1     Processing and Properties of Intermetallic Matrix Composites
Principal Investigator:      R. Abbaschian

Section 2     Mechanical Alloying of $MoSi_2$
Principal Investigator:      M.J. Kaufman

**BOOK III**

Section 1     Processing of Ceramic Matrix Composites
Principal Investigator:      M.D. Sacks

Section 2     Processing of $BaO-Al_2O_3-2SiO_2$ Fibers
Principal Investigator:      D.E. Clark

**BOOK IV**

Section 1     Processing and Mechanical Property Characterization of Tape
Cast, Multilayer, Alumina/Nickel Laminated Composites
Principal Investigator:      J.J. Mecholsky

| Accesion For | | |
|---|---|---|
| NTIS CRA&I | | ☒ |
| DTIC TAB | | ☐ |
| Unannounced | | ☐ |
| Justification | | |
| By | | |
| Distribution / | | |
| Availability Codes | | |
| Dist | Avail and / or Special | |
| A-1 | | |

# BOOK IV

# Section 1

# Processing and Mechanical Property Characterization

# of

# Tape Cast, Multilayer, Alumina/Nickel

# Laminated Composites

**Principal Investigator:**     **J.J. Mecholsky**

# PROCESSING AND MECHANICAL PROPERTY CHARACTERIZATION OF TAPE CAST, MUTILAYER, ALUMINA/NICKEL LAMINATED COMPOSITES

Zheng Chen and J. J. Mecholsky, Jr.

## ABSTRACT

Ceramic laminated composites were designed in order to increase the strength and toughness of alumina structures. This was accomplished by strategic placement of several ductile layers in the alumina ceramic. This placement served to arrest cracks and produce a residual compressive stress field in the alumina layers in order to prohibit crack initiation and propagation. This composite has a hard surface that is reasonably strong, possessing chemical inertness and thermal stability. A tape casting technique was used for fabrication and subsequent hot pressing was used for densification. Tape-casting makes it feasible to arrange different materials layer-by-layer at strategic locations and select the optimized thickness of each layer in order to achieve the mechanical and chemical properties of the composites that are unattainable by conventional methods of fabrication.

Systematic study of the mechanical behavior and failure characteristics of the laminated composites included study of the influence of thickness of the constituent layers and interfacial conditions on the strength and toughness behavior, the mechanisms of toughening and strengthening, the influence of flaw size on the strength of the composites, and the tolerance to thermal shock damage. The results of this research indicate the following:

1. Tape casting and subsequent hot pressing can be successfully exploited to fabricate alumina/nickel laminated composites.

2. Toughness and strength of the laminated composites can be controlled by interface design.

3. The apparent toughness and strength of the laminated composites were increased to above 10 $MPm^{1/2}$ and 700 MPa, respectively.

4. The strength of the laminated composites are nearly insensitive to flaw size and a noncatastrophic failure characteristic shows an improvement in the reliability over monolithic alumina.

5. Tolerance to thermal shock damage shows that these laminated composites appear to be good candidates for damage tolerant materials.

TABLE OF CONTENTS

# SECTION 1

## INTRODUCTION

Ceramics are materials "which have as their essential component, and are composed in large part of, inorganic nonmetallic materials."[1-3] In comparison to metals, ceramics possess many properties which are desirable for materials used in industrial applications: high strength, low density, and excellent chemical and thermal stability. In particular, alumina exhibits nearly constant strength over a broad temperature range ($\leq 1000°C$), high hardness (18.1 GPa), low density (3.98 $g/cm^3$), and high oxidation resistance.[1,2] Therefore, alumina is used in many commercial structural applications such as microelectronic substrates, spark plugs, cutting tools, armor, prosthesis and actuators.

Unfortunately, as with many other ceramics, alumina also shows brittle fracture behavior (low fracture toughness, $K_{Ic}$ =2.8 to 3.5 $MPam^{1/2}$) and low thermal shock resistance ($\Delta T_c$ = 200 °C).[2] The strength of monolithic alumina is especially sensitive to flaw and defect size, and a low ability to resist crack propagation.[2] It is this lack of stress-relieving characteristics which gives alumina its low tolerance to flaws and defects, causes catastrophic failure during applications, and limits the full commercial utilization of its desirable properties. Many researchers have attempted to solve these problems by forming composites which exhibit toughness values that are much greater than monolithic alumina.[3,4,5,6,7]

One type of ceramic matrix composite system which has been studied is the ceramic-metal system. The fracture behavior of a ceramic matrix containing a metal particulate phase has been studied by several authors.[8,9] In these particulate composites, the metal particles have been observed to cause crack deflection and crack bridging as the crack propagates through the material. In general, such crack-particulate interactions result in measured toughnesses and strengths which are greater for the composite than for the monolithic alumina. However, the surface hardness and chemical stability of the ceramic are usually inferior to the parent matrix because the surface contains soft and relatively low oxidation resistant metal particulates.

The goal, then, is to develop a ceramic/metal composite which has high strength and

1

resistance to crack growth, has a hard surface that is reasonably strong, and possesses chemical inertness and thermal stability. One of the ways to achieve this goal is to insert several ductile (tough) layers in the brittle material to stop or blunt any cracks and to produce a residual compressive stress field in the ceramic layers in the longitudinal direction to prohibit or at leastinhibit crack initiation and propagation. Laminated composites combining brittle and ductile layers were successfully used in polymer-matrix composites for many years.[10] Even though ceramic multi-layer materials comprised of alternate layers of ceramics with metals have been already manufactured, the applications have been limited mostly to ceramic capacitors and microelectronic substrates.[11] Most recently, the fracture behavior of a ceramic matrix composite containing several ductile metal layers was studied, which showed that ceramics can be toughened by inserting ductile layers, because the ductile layers serve to arrest and bridge advancing cracks in the brittle layers which increases the reliability of the composites.[12,13] However, the application of ceramic laminates is often limited by several problems:[14,15] first, cracks are often initiated in ceramic layers near or along the ceramic/metal interface due to thermal expansion mismatch; second, delamination frequently happens near the edges because of both thermal expansion and elastic mismatch; third, most of the ceramic/metal bonds are formed by hot pressing of these two solid layers (ceramics/metals). It is very difficult to eliminate interface flaws which result from this processing procedure. The existence of these cracks in the ceramic layers causes limitation of strength of laminated composites.

Tape-casting techniques,[16,17] which are commonly used in the electronics industry, can be adapted to produce metal tapes as reinforcement/toughening layers in a manner analogous to that used in manufacturing polymer composites. Moreover, tapecasting makes it feasible to arrange different materials layer-by-layer at strategic locations and select the optimized thickness of each layer in order to achieve the mechanical and chemical properties of the composites that are unattainable by conventional methods of fabrication. Therefore, the tape-casting technique was selected to produce alumina/nickel laminated composites with selected layers intentionally introduced at strategic locations to arrest and bridge cracks and control residual compression in the ceramic layers using thermal expansion mismatch. This strategy was intended to result in a tough, strong, and high reliability composite.

2

Nickel (fcc crystal structure) was selected as the toughening material in this laminated composite. Nickel possesses relatively high temperature strength, relatively good oxidation and corrosion resistance, a high hardening rate, and a high thermal expansion coefficient.[18] These properties are combinations of what we desire in designing this type of laminated composite.

The objectives of this investigation were accomplished by studying three distinct subjects which are interrelated: toughening using metallic lamina, interface design of multilayer structure, and thermal shock resistance. These areas are discussed and presented as technical journal papers in Chapters 3, 4, and 5, respectively. The details of the processing of these composites will first be presented in Chapter 2. The following paragraphs outline the content of Chapter 2, 3, 4, and 5.

The main effort in fabrication of these composites was to exploit a process to produce alumina and nickel sheets using tape casting techniques and to form a bond between the alumina/nickel layers during their densification under hot pressing in order to achieve defect free interfaces. Slurry preparation, tape casting, lamination, binder burn-out, and hot pressing procedures were investigated for this specific application and are presented in this chapter.

In this Chapter 3, the mechanical behavior of the laminated composite was characterized using different methods i.e., indentation strength and chevron notch beam techniques. The variation of layer thickness on the strength and toughness of the composites was studied. Moreover, in order to investigate the sensitivity of strength to surface flaw size, different sizes of flaws were introduced in the surface using a Vickers indenter. The results show this type of laminated composite to be a good candidate for damage tolerant composite design.

Bonding conditions have a great influence on the plastic behavior of bonded ductile materials which, in turn, directly affect the increment of toughness and strength of laminated composites. This Chapter 4 discusses the interface design of alumina/nickel bonds by physically changing the tortuosity of the interface in order to vary the strength of bonding. A bonded single nickel layer model was used to study the variation of plastic behavior of the nickel layer for different bonding conditions. The results were used to design alumina/nickel

3

laminated composites whose toughness and strength can be controlled by control of the interface design.

Since most applications invariably involve rapid environmental temperature variations and high heat transfer, it is important to investigate the thermal shock resistant capacity of the laminated composites. A wide range of quenching temperature differences ($\Delta T = 150$ to $1200$ °C) was used to measure the retained strength of laminated composites which were quenched into room temperature water. The results compare to that of monolithic alumina and show an improvement in the thermal shock resistance capacity of the composite. The reasons causing this improvement were also investigated and are reported in this Chapter 5.

# SECTION 2

## PROCESSING OF LAMINATED COMPOSITES

Tape casting basically involves the suspension of finely divided inorganic powders in aqueous or nonaqueous liquid systems. These systems are comprised of solvents, binders, plasticizers, and other additives to form a slip that is cast in thin, relatively large area sheets. In the tapecasting process currently used in development of ceramic/metal laminated composites, the ceramic powders and metal powders are mixed with a liquid organic binder, respectively, to produce slurries with well dispersed particles. The slurry is then cast under a doctor blade to spread a thin layer on a continuous moving film of plastic (Mylar). The tape is air dried to a flexible sheet that can be cut to size for use as a constituent layer in a laminated composite. Various mechanical properties can be achieved by specifying the precise sequence of layer location and composition. The processing procedure for fabrication of the laminated composite consisted of material selection, slurry preparation, tape casting, lamination, binder burn-out, and hot pressing as schematically shown in Figure 2-1.

### 2.1 Materials

For tape casting, a powdered form of nickel and alumina is required. In this research, Johnson Matthey nickel powder (10256) and Reynolds alumina powder (RC-HP DBM) were used, the composition of nickel and alumina is listed in Table 2-1. The size distribution of powder was characterized using a Horiba CAPA-700 Particle Analyzer, and cumulative mass percent larger-particle size plots are shown in Figure 2-2. Most particles are smaller than 0.5 $\mu$m for alumina and 7 $\mu$m for nickel. The particle shape is very irregular as shown by SEM pictures in Figure 2-3.

### 2.2 Slurry Preparation and Tape Casting

The MSI's B-73305 substrate binder was used in all of this research. Different amounts of toluene was added to adjust slurry viscosity. An attempt was made to minimize the amount of binder in the alumina or nickel slurry while maintaining a suitable condition of high slurry viscosity and final tape strength. About 40 wt% and 20 wt% B-73305 was added to the powders to make alumina and nickel slurries, respectively. This combination was found to

make the best constituent of slurry for forming good tapes, which have high green density, for subsequent laminating. The viscosity of each slurry was measured using a Brookfield-Digital Viscometer and plots of viscosity versus shear rate are shown in Figure 2-4. All slurries were ball-milled about 20 hours prior to casting. After being filtered by a 53 $\mu$m nylon Macro filter, the slurries were then tapecast onto a Mylar carrier tape that travels into a dry chamber at about 3 m/min using an INCETEK Model 104 tapecaster. The final dried tape thickness is approximately 80 $\mu$m. Green tape SEM pictures (Fig. 2-5) show that both powders were well dispersed in the binder and no aggregated particles were observed. Moreover, the pictures also exhibit that dense green compacts of alumina and nickel powders can be packed by tape casting techniques. All these tapes were relatively easy to handle and were sectioned into 50 mm diameter circles using a stainless steel punch designed for this project. Laminated composites were constructed from these tapes.

Table 2-1.    Composition of alumina powder and Nickel powder

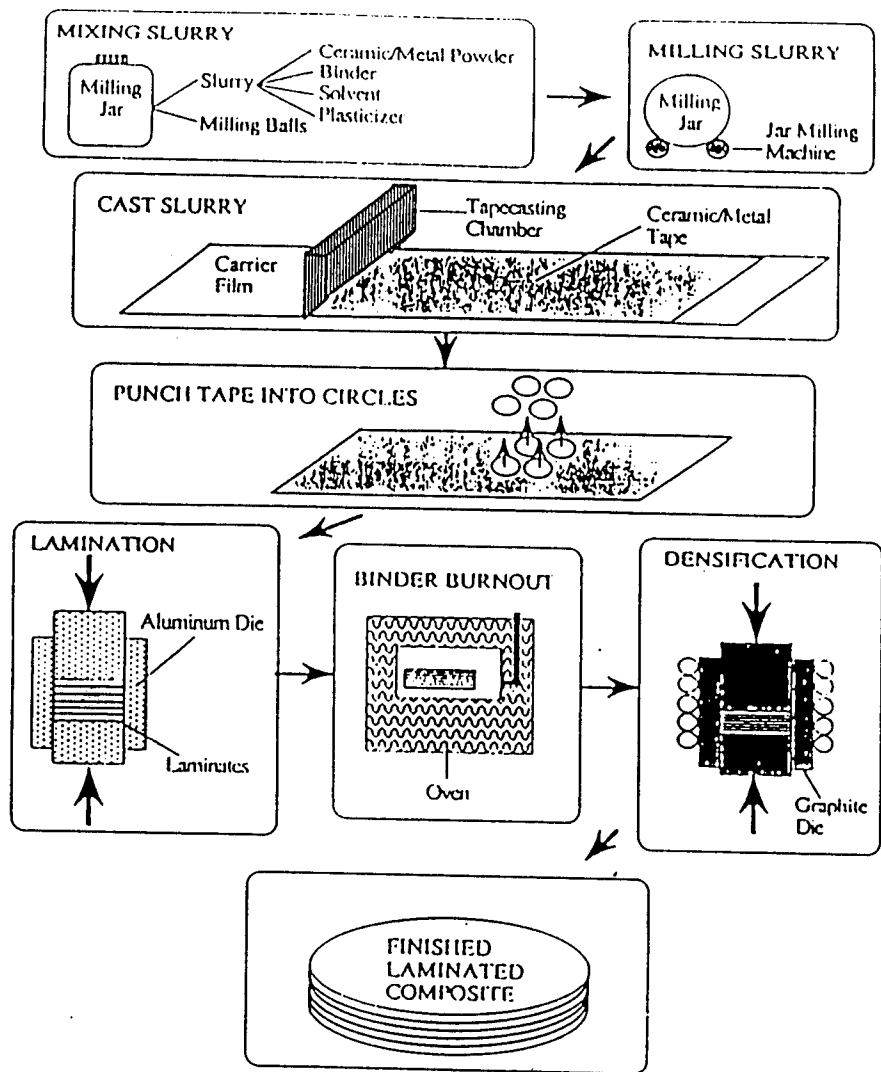| Alumina (RC-HP DBM) | | Nickel (10256) | |
|---|---|---|---|
| Element | wt % (PPM) | Element | wt % |
| Na | 66.0 | Ni | 99.9 |
| Si | 20.1 | C | <0.1 |
| Fe | 35.0 | | |
| Ca | 60.0 | | |
| Ga | 33.5 | | |
| Mn | 0.8 | | |
| Mg | 310.0 | | |
| Zn | 14.5 | | |
| Cr | 2.7 | | |
| Ti | <0.6 | | |
| Li | 0.5 | | |
| B | 1.2 | | |
| Zr | 0.7 | | |
| Cu | <1.2 | | |
| Ni' | 1.6 | | |
| Be | 0.4 | | |
| V | <0.6 | | |
| K | 1.0 | | |

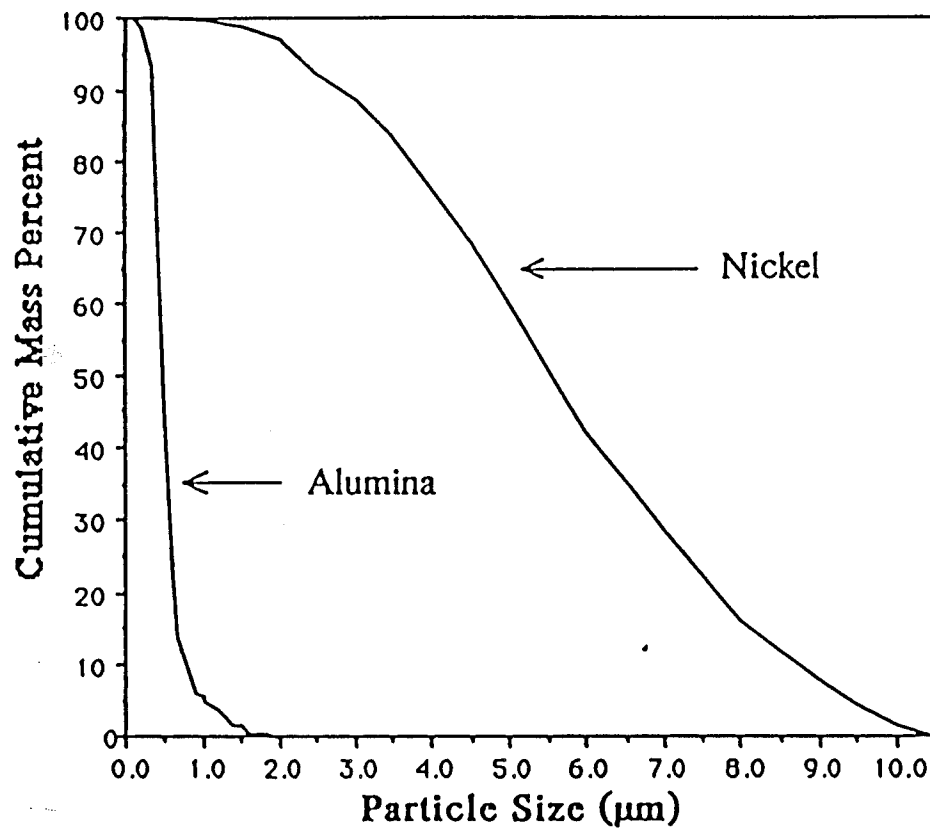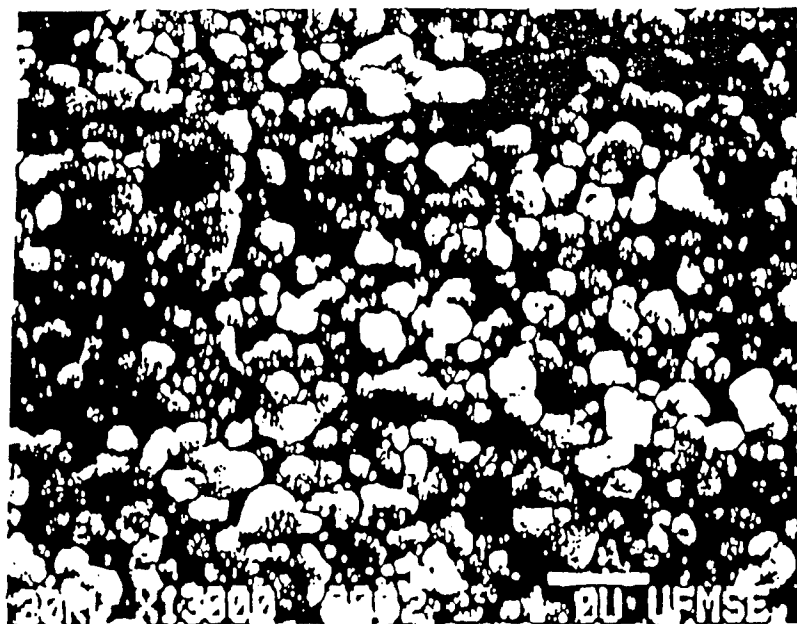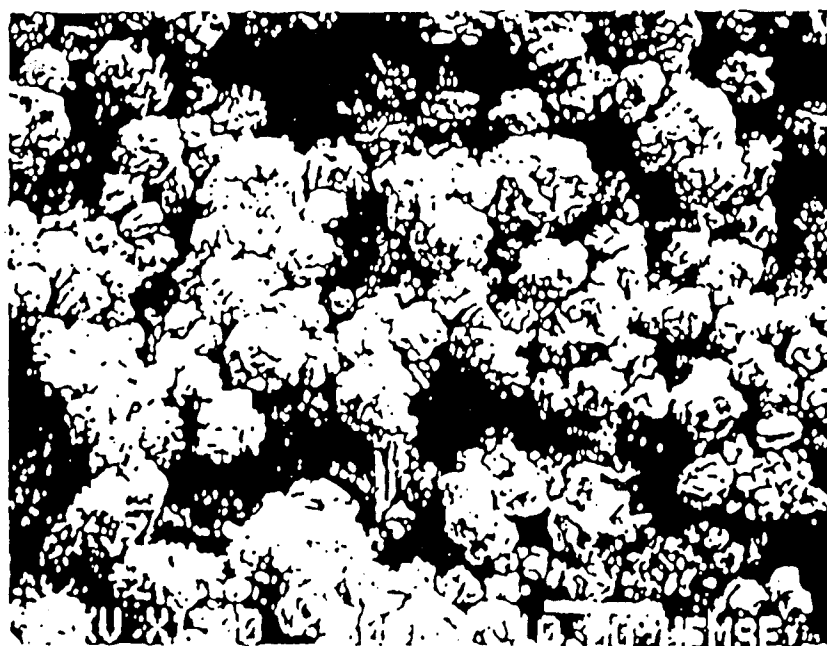**Fig. 2-1** Schematic processing flow chart.

Fig. 2-2 Cumulative size distribution of Alumina powder and Nickel powder.

(A)



(B)

**Fig. 2-3** Scanning electron micrographs show the shape of alumina particles (A) and Nickel particles (B).
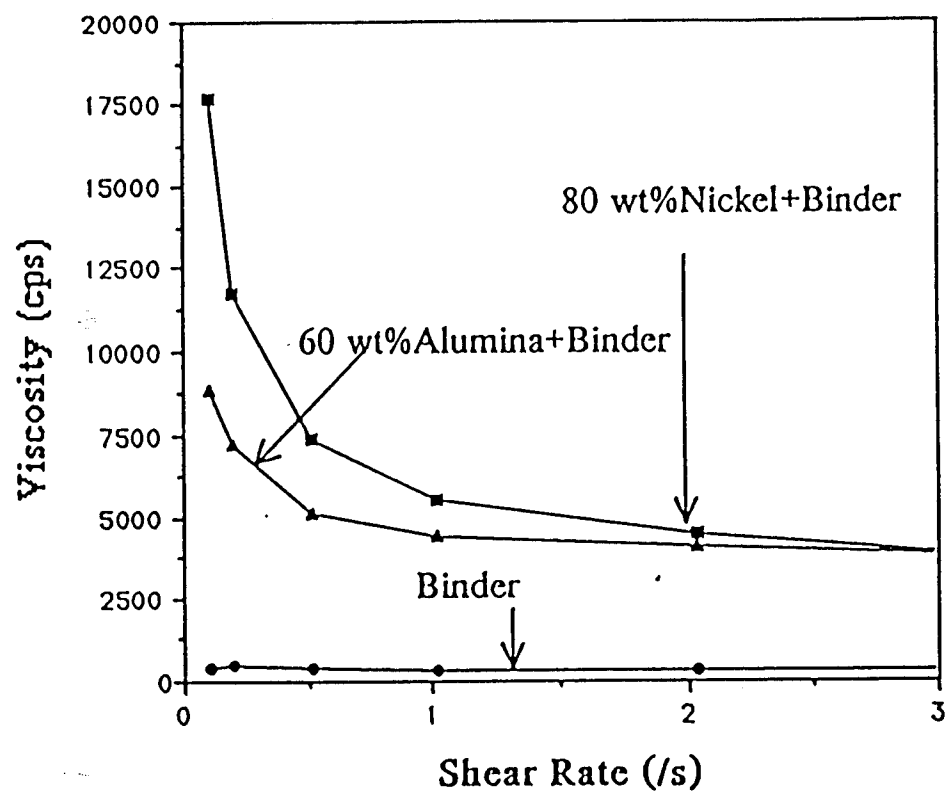
**Fig. 2-4** Viscosity shows a function of shear rate for alumina binder and Nickel binder, respectively.

11

## 2.3 Lamination

The circle tapes were laminated under heat and pressure using a stainless steel punch and aluminum die. The green laminates were produced at a pressure of about 75 MPa, at temperatures around 80 °C. Lamination time is typically 10 minutes. The green laminates showed good strength and fairly good flexibility using this laminating schedule so that they can be easily handled. A schematic lamination process is illustrated in Figure 2-5.

## 2.4 Binder Burn-out

It was necessary to remove the polymer binder from the green laminates prior to sintering to prevent contamination of the hot pressing furnace used to densify the parts and to avoid porosity. The polymer removal (burn-out) was accomplished by heating the green laminates at a controlled rate to a specified temperature. The temperature is selected such that the binder starts to degrade and to be removed from the laminates. The thermogravimetic analysis (TGA) and differential thermal analysis (DTA) were used to study the relationship between the reaction rate of binder with the atmosphere and elevated temperature, and to find the temperature at which the binder starts degradation on a Harrop ST-736 Simultaneous Differential Thermal Analyzer/Thermogravimetric Analyzer. According to the TGA and DTA curves (Fig. 2-7), a strong binder degradation reaction occurs from 280 to 400 °C. After 400 °C, even though the reaction proceeds, the rate becomes slow. After considering the minimization of nickel oxidation and the maximization of binder degradation and contiguity of the green laminates, binder burn-out cycles were determined as shown in Figure 2-8. This operation is performed at atmosphere in an unsealed furnace, and almost all the binder was successfully removed from the laminates.

Even though nickel is a relatively high oxidation-resistant element which does not show oxidation when it is heated up to 600 °C for 4 hours in the TGA and DTA testing, the high surface area inherent in green tape and the long time exposure to atmosphere during the burn-out cycle increases its susceptibility to oxidation. The nickel tapes after burn-out showed partial oxidation of the nickel particles. According to the X-ray diffraction spectrum (Fig. 2-9), a small amount of NiO was formed. Therefore, an additional step is needed to reduce the NiO into Ni before full densification of the green laminates. This step was successfully carried out

12

by heating up the laminates to 800 °C for 1.5 hours in a reduced atmosphere before hot pressing. The follow-up X-ray diffraction spectrum shows no NiO remaining in the nickel layer and only Ni peaks in the spectrum (Fig. 2-9). The laminates after burn-out are relatively weak and careful handling is required.


## 2.5 Hot Pressing

The densification of the green laminates was performed in a vertical hot press furnace (Centorr Model) which is heated by an induction coil. The green laminate was covered by graphite foil and mounted into a graphite die (50 mm of inner diameter). The hot press die assembly is schematically shown in Figure 2-10. In order to achieve fully dense monolithic alumina, as high as possible hot pressing temperatures are desired. However, for $Ni/Al_2O_3$ laminates, this temperature should be below the 1450 °C (nickel melting point). After a series of trial runs, about 1350° C was selected as the hot pressing temperature (measured at die surface). The hot pressing schedule is illustrated in Figure 2-11. A reducing atmosphere was applied before pressurization during hot pressing in order to reduce the oxygen in the nickel layer (in the form of NiO) which was produced during the binder burn-out cycles. The density of the hot pressed monolithic alumina was 3.99 $g/cm^3$ measured by the Archimedes submersion method.


Alumina/nickel laminated composites were successfully fabricated by this processing procedure and used to test their mechanical behavior.

13
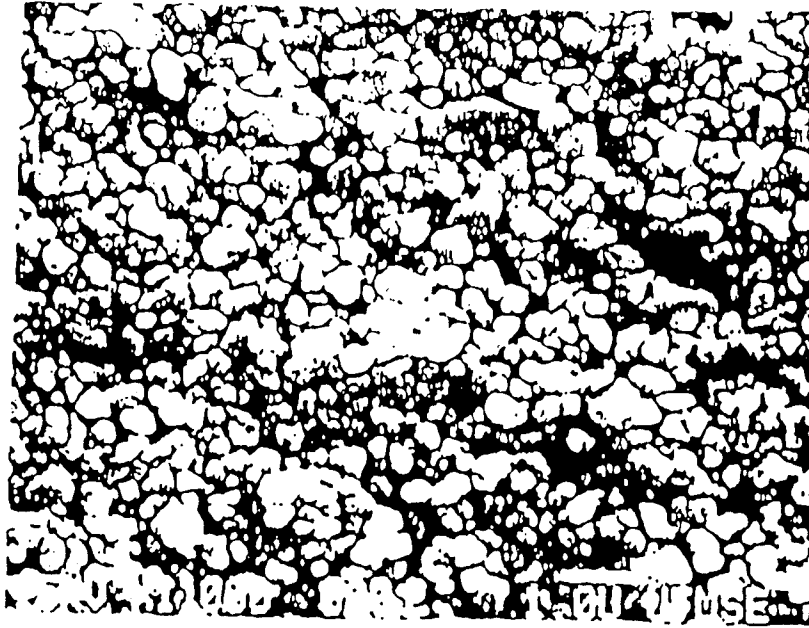
(A)
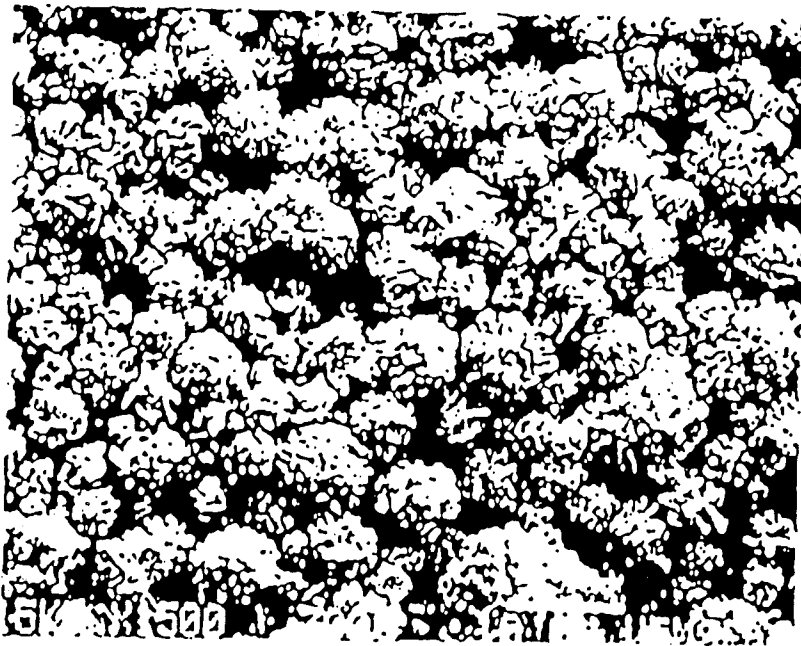


(B)

Fig. 2-5 SEM pictures show Alumina particles (A) and Nickel particles (B) are well dispersed in B-73305 binder and formed in a good green compact by tape casting.
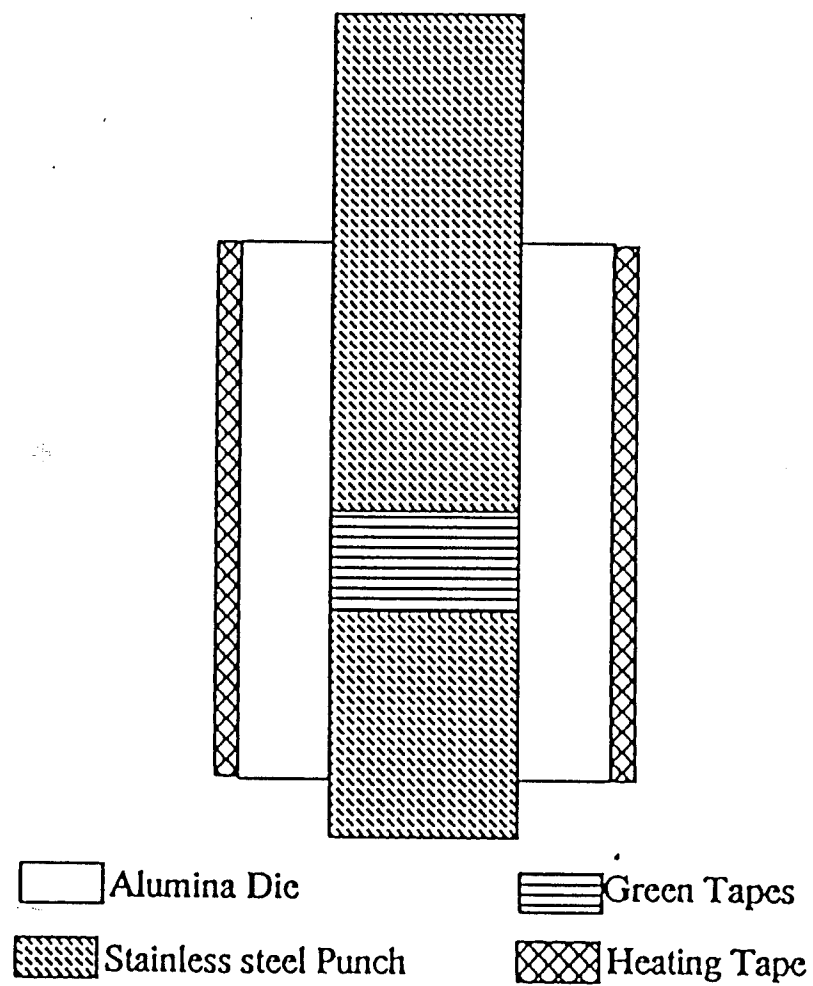
Fig. 2-6 In laminating, stacked tapes are loaded in a die, heated, and pressed to form a green laminate.
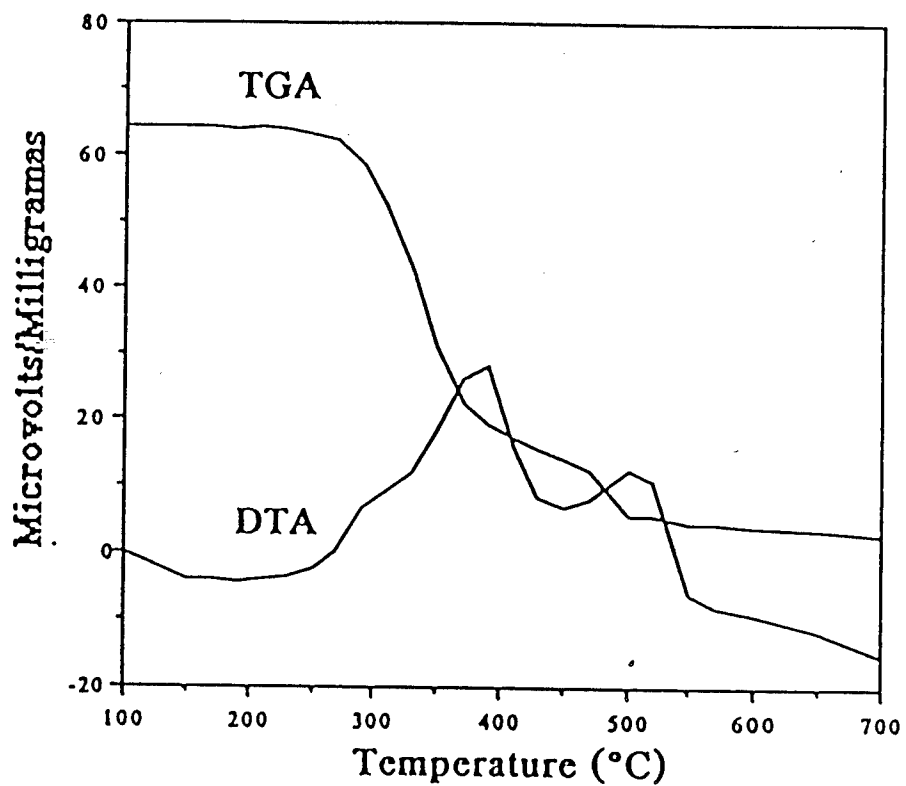
**Fig. 2-7** Thermogravimetric and Differential Thermal analysis curves indicate binder weight loss and differential temperature of binder degradation versus temperature.

Fig. 2-8 Schematic Binder Burn-Out Cycle

17

Fig. 2-9 X-ray diffraction patterns correspond to the nickel tape after reducing reaction (A) and the nickel tape after burn-out cycle (B). C, and D are JCPDs patterns for Ni and NiO, respectively.

18

Fig. 2-10  A Schematic Hot Press Die Assembly

Fig. 2-11 Schematic Hot Pressing Schedule

# SECTION 3

## TOUGHENING AND STRENTHENING BY METALLIC LAYER IN ALUMINA/NICKEL LAMINATED COMPOSITE

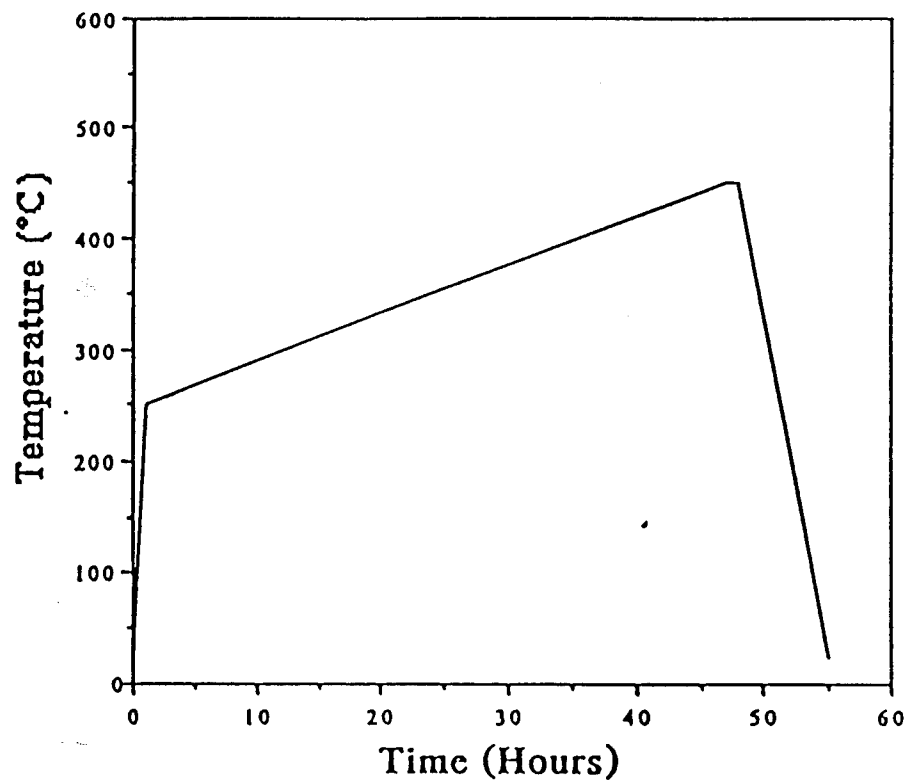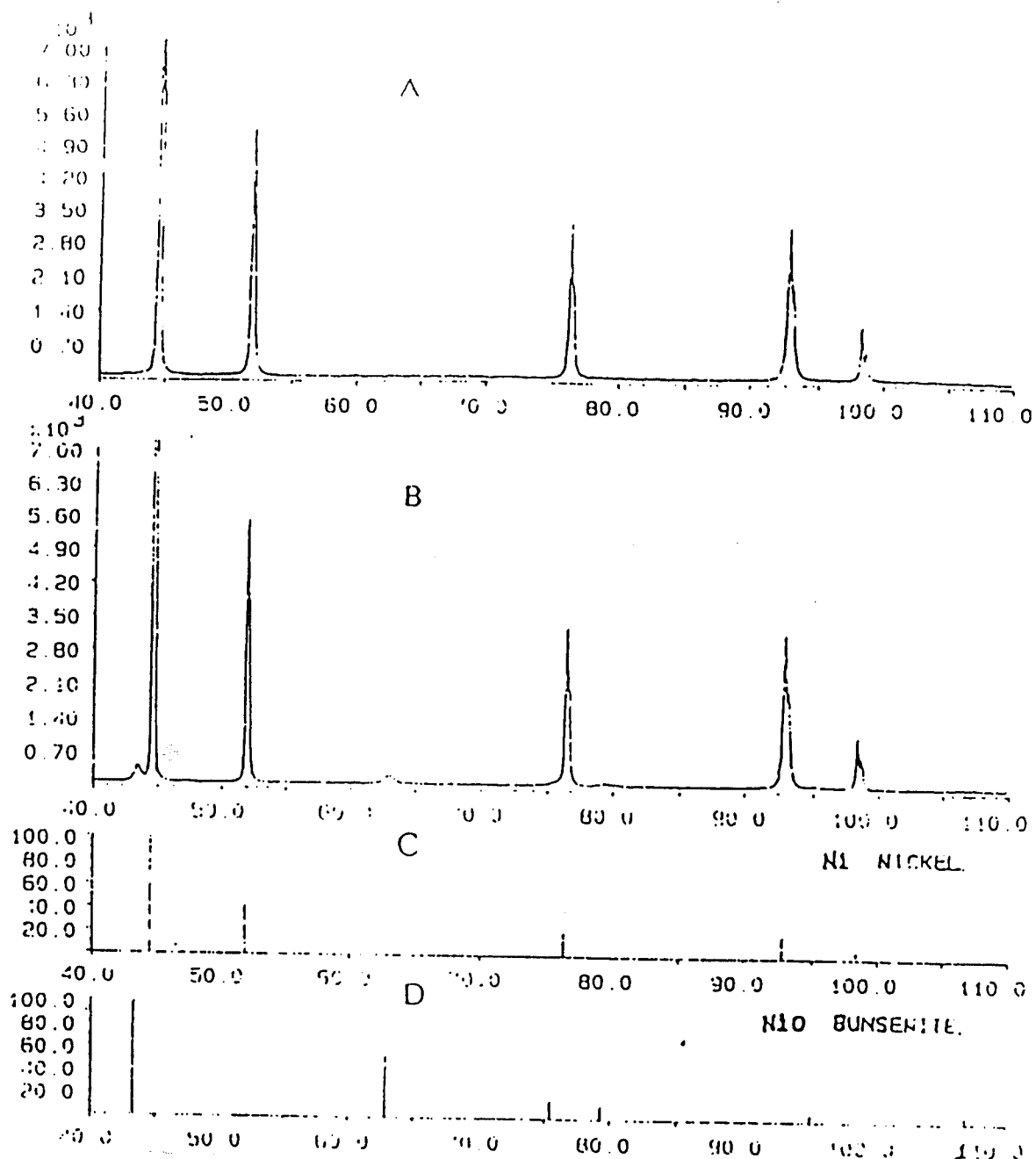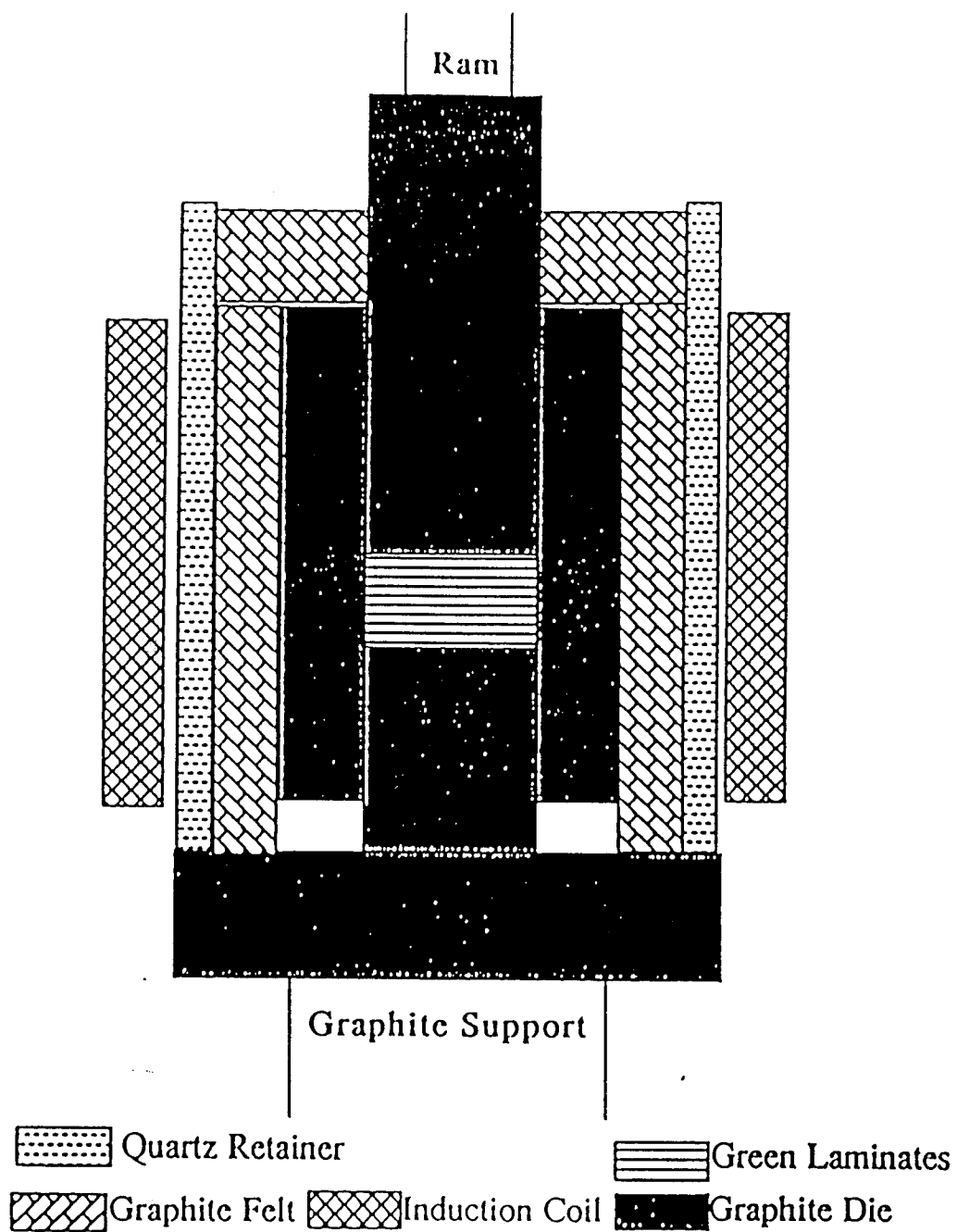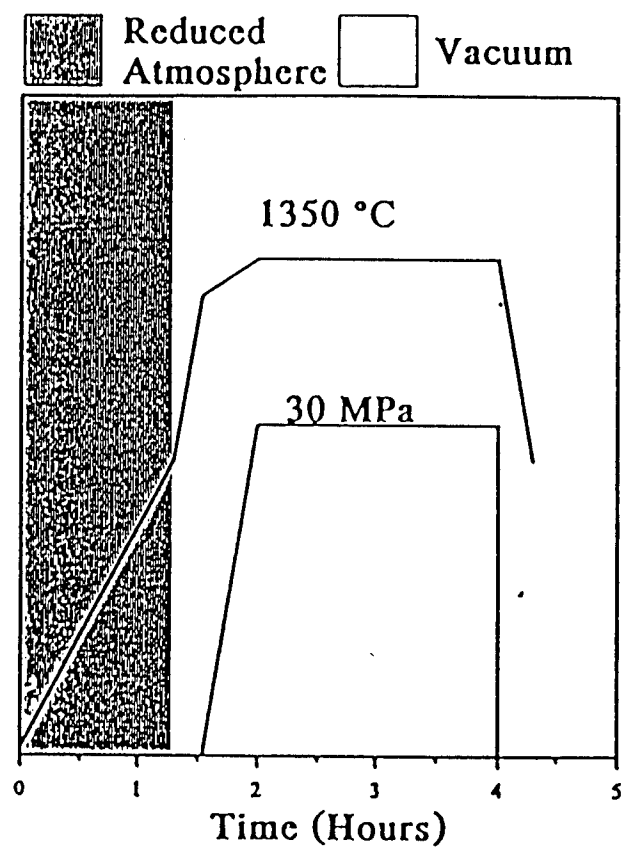### 3.1 Informations and Review of Works On Toughening Brittle Materials

The strength, $\sigma$, of most ceramics depends on the flaw size, a, by the simple application of fracture mechanics:[19]

$$\sigma = \frac{YK_{Ic}}{\sqrt{a}} \qquad (3\text{-}1)$$

where Y is a well-documented parameter of crack and specimen geometry, $K_{Ic}$ is the critical stress intensity factor, i.e., a measure of the toughness of the material. Although elimination or control of flaw size during materials processing has been greatly improved,[20,21] flaws (cracks) are still induced during application. The objective of research for structural applications is to generate ceramics having high reliability. One of the means of achieving high reliability is to produce materials that have flaw insensitive strength and non-catastrophic fracture.[22] To achieve this objective, one of several approaches has been studied here: ductile phase toughening.[23,24,25,26,27] This toughening mechanism is based on ductile phase bridging of cracks in a ceramic matrix. This bridging is associated with crack trapping or shielding and energy dissipation in the formation of a plastic zone and interface debonding.[22,28] As the crack extends in a ductile phase reinforced ceramic matrix composite, the toughening increase comes mainly from the amount of energy dissipated. Of course, the residual stresses, which are caused by thermal expansion mismatch, also are capable of suppressing crack propagation due to a residual compressive stress field around the crack tip.[29,30] However, for most discontinuous ductile phase reinforcing ceramics in which the ceramic phase is continuous, the residual stress does not contribute to a large increase in toughness. Thus, ductile phase bridging and the effect of the plastic zone size provide the major increase in toughness.[22,31] Since most ductile phases are metals or their alloys, there are two major drawbacks caused by the addition of soft ductile phases to the external surface of ceramics: one is decreasing the wear-resistance of the ceramic by decreasing the hardness of the surface; another is that the

ductile phase on the surface could be corroded more easily in the severe chemical environment to form "pits", which could be a source of failure.

Is it possible to use ductile phase toughening to reinforce ceramics and not sacrifice the potential of wear-resistance and chemical stability of ceramics? This article is based on this question and proposes using metallic lamina to toughen and strengthen the ceramic layer in nickel/alumina laminates which are made by tape casting and hot pressing techniques. In this case monolithic ceramic layers are arranged as the outside layers (external surface) and ductile (metal) layers are beneath the ceramic in order to retain the high wear resistance and high chemical stability of the surface [Fig. (3-1)]. Moreover, the magnitude and orientation of the residual stress field in the alumina layers can be controlled.

Classical laminated plate theory can be used to calculate the properties of ceramic-composite laminates using their constituent properties.[32] Also, it can guide the material designer to tailor laminates by specifying the precise sequence of lamina position and composition to obtain materials with desired characteristics. Accordingly, Amateau and Messing[33] took advantage of this analysis by using surface residual compression induced by thermal mismatch due to different amounts of SiC-wiskers in an alumina matrix to toughen ceramic-based hybrid laminates. In other studies, Evans and Ruhle[31] and Cao et al.[34] found that quasi-static cracks located at the interface in a ceramic/metal bonded system exhibited crack blunting. They also predicted the plastic zone profile in the ductile layer during thermal and mechanical loading and found that the plasticity profoundly affects several aspects of mechanical behavior in ceramic/metal bonded systems.

However, the application of metal/ceramic laminates as structural materials is often limited by the bonding between the two materials. This bonding invariably results in stress concentrations which may initiate cracks from the bonded region and cause failure, and eventually, limit the strength and toughness of laminates.[35] Even though Au and Pt can be used to form a bond to limit the stress concentrations and blunt cracks because of the local large plastic deformation in the soft layer, this approach has limited practical utility because

interface flaws still can not be easily eliminated.[36] The tape casting technique provides a good opportunity to bond ceramic with metal very successfully through lamination followed by hot pressing or sintering. This technique is presented here with pure nickel lamina as the toughening reinforcement for alumina layers.
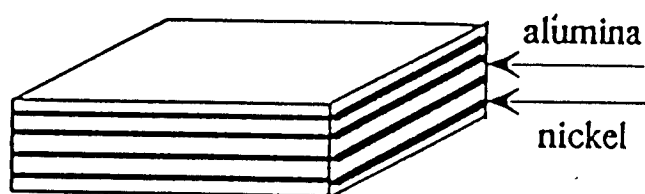
alumina

nickel

**Fig.3-1.** Schematic of metal/alumina alternate laminates

## 3.2 Experimental Procedure

### 3.2.1 Materials and Processing

The laminates consist of alternate layers of pure nickel* and alumina** powders which were mixed with polyvinyl alcohol based binder. The layers of both materials are made by tape casting and bonding to each other through intermediate layers to form green laminates. Then, the green laminates were heated up about 450 °C for 50 hours in an air atmosphere for binder burn-out. Finally, the green laminates are densified to a laminate plate 50 mm in diameter by hot pressing around 1350 °C. The intermediate layer is designed to have a thermal expansion coefficient between the nickel's and alumina's coefficients in order to limit the stress concentration along the interface and form a strong bond. The laminates are formed at high temperature and then cooled down to room temperature. Thus, the alumina layers are left in a state of residual compression and the nickel layers should be left in a state of residual tension in the longitudinal direction parallel to the interface[37] because alumina layers have a smaller thermal expansion coefficient ($8.24 \times 10^{-6}$ /°C) than the nickel layers ($13.3 \times 10^{-6}$ /°C). It is preferable to have both outside layers to be alumina, since longitudinal compressive residual stress helps to prevent crack initiation on the surface and propagation through the cross section. In addition, the alumina has high wear-resistance and chemical stability as an external surface. So, the laminate plate is designed to have an odd number of alumina layers in a self-equilibrating condition.

### 3.2.2 Strength, Hardness, and Toughness Measurements

Flexure strength tests were made with non-initiated flaws and with pre-indented cracks which were induced using a Vickers diamond indenter. The thickness and width of specimens are listed in Table 3-1. All specimens were 25 mm long, cut from the laminated plates and

---

* Johnson Matthey, P.O. Box 8247, Ward Hill, MA 01838-0747
** Reynolds, P.O. Box 97, Bauxite, AR 72011

polished down to 1 $\mu$m [Fig. 3-2]. All specimens were tested on a tensile testing machine*, at a crosshead rate of 0.078 mm/min. The hardness was calculated using:[38]

$$H = \frac{2P\sin(\theta/2)}{L^2}$$

(3-2)

where H is hardness, P is indent load, L is diagonal length of indent impression, and $\theta$ is the angle between the diamond faces(136°). Toughness was measured using a chevron-notched beam [Fig. 3-2c] 4.5 mm thick (W) by 4.4 mm wide (B) by 25 mm long. The notch length $a_o$ and $a_1$ are 0.2 mm and 3.7 mm respectively, i.e., $\alpha_1(= a_1/W)$ is 0.822 and $\alpha_o(= a_o/W)$ is 0.044. The tests were made on a tensile testing machine** at 0.05 mm/min crosshead rate. The fracture toughness, $K_{Ic}$, is evaluated at the maximum load (Pmax) and minimum Y* :

$$K_{Ic} = \frac{P_{max}Y^*}{B\sqrt{W}}$$

(3-3)

The compliance function, Y*, can be derived from the Bluhm slice model.[39] The Y* value is obtained by curve fitting,

$$Y^* = (3.08 + 5.00\alpha_o + 8.33\alpha_o^2)\frac{S_2 - S_1}{W}[1 + 0.007(\frac{S_1 S_2}{W^2})^{1/2}(\frac{\alpha_1 - \alpha_o}{1 - \alpha_o})]$$

(3-4)

where all the parameters are specified in Fig. 3-2c. In our case, Y*=7.50. All the specimens were tested in four-point bending using a minor span $(S_1)$ of 10 mm and a major span $(S_2)$ of 20 mm. Specimens with non-initiated flaws were tested to determine strength variations of laminates with variation in the thickness of nickel layers. The specimens with initiated flaws were tested to examine how the flaw size and the residual stress affects the strength of laminates. All the results were compared to monclithic alumina specimens. The fracture specimens have been examined using scanning electron microscopy.

---

* Mold 810, MTS Corp., P.O. Box 24012, Minneapolis, Minnesota 55424.
** Mold 1125, Instron Corp., 100 Royall Street, Canton, Massachusetts 02021.

## 3.3 Results and Discussion

### 3.3.1 Flexure Strength

The flexure strength of the alumina layer was calculated based on the formulas given by Hashin and Rosen (in Appendix) for composite laminates,[32] and shown in Table 3-1. No evidence showed that interface debonding occurred with the crack initiated along the interface before the crack initiated on the surface of the first alumina layer. The fracture surface clearly shows the crack was initiated on the tensile surface and then propagated toward the inside layers. The load-deflection curves [Fig 3-3] exhibit an abrupt load drop at the load which initiates the crack, then the load drop stops at a level dependent on the thickness of nickel layer. This phenomenon is attributed to the nickel reinforcing layer bridging between the crack surfaces after the crack is initiated. The bridge stops or slows crack propagation. This process of bridging eliminates catastrophic failure which is usually seen in most ceramics. As the crack further extends under the loading, the nickel layers are stretched and necking begins between the crack surfaces. Eventually, failure of the nickel layers occurs by ductile rupture; the difference of fracture path between the laminates and monolithic alumina is shown in Fig. 3-4. Fig. 3-5 shows ductile ridge marks and dimples in the nickel layer fracture region. Large plastic strain occurs in the ductile layers and the regions between the crack surfaces cause large stress constraints[13] in the interfaces adjacent to the major crack [Fig. 3-4]. Local debonding [Fig.3-4] is initiated in order to reduce the constraint and increase the plastic deformation prior to the ductile layer failure. Plastic dissipation and the creation of new fracture surface produced by debonding the interface provides large increases in the toughness of laminates. The toughness results will be shown in a later section. The flexure strength results of the alumina layer in the composite [Table 3-1] was increased about 50 percent over that of monolithic alumina, but thickness changes in the nickel layer from 125 $\mu$m to 240 $\mu$m do not display much influence on the flexure strength. The hardness values of the surface layer in the laminates exhibit the same values as the monolithic alumina [Table 3-1]. However, the fracture energy which can be obtained from the area under the load-deflection curve does increase with increasing thickness of the nickel reinforcing layer.

27

### 3.3.2 Flaw Size and Toughness

The strength of most ceramics and many particulate composites depend on the critical flaw size at fracture and can be calculated based on fracture mechanics [eq.(3-1)].[23,24] Even though many approaches have been developed recently to eliminate large flaws during processing, abrasion or impact, in-service applications can produce large flaws or enhance small flaws. Thus, the strength of most ceramics is statistical. The influence of flaw size on strength was tested with Ni(180) specimens, which were intentionally indented to produce cracks on their tension surface [Fig. 3-3b] using a Vickers diamond indenter and broken in four-point bending. The results are shown in Fig. 3-6 which contain a graph of the log(strength) vs. log(indent load). For monolithic alumina, the strength decreases with increasing flaw size with a slope of "-1/3" as expected.[40] However, unlike the monolithic alumina, the strength of the laminates only drops about 17 percent when the flaw size [2b] (surface trace) varies from 50 $\mu$m to 410 $\mu$m and indicates that the strength is fairly insensitive to the flaw size. Much more resistance to crack propagation is shown in the laminates than in monolithic alumina from indentation strength results. This improvement is attributed to the residual compressive stress in the outer alumina layers and crack blunting by the ductile layers. If we use a Modified Cook and Lawn formula:[41]

$$K_c = \zeta \sigma \sqrt{c_m}$$

(3-5)

where $K_c$ is a measure of the toughness*, $\zeta$ is a geometrical constant equal to 1.65 in this case, $\sigma$ is the flexure strength, and $c_m$ is the critical flaw size of an equivalent semi-circular crack, we obtain a curve [Fig. 3-7] in which $K_c$ of the laminates increases as the initial crack size increases, i.e., "R" curve behavior.

In order to obtain the large crack limit, another approach was applied to determine the toughness of the laminates: four-point-flexure specimens using Chevron notches. The toughness values (eq. 3-3) of both laminates and monolithic alumina are listed in Table 3-2. The toughness of monolithic alumina agrees very well with that measured by the Cook and

---

* $K_c$ is used here because it is determined from indentation cracks rather than other techniques. However, for practical poposes' $K_c \approx K_{Ic}$.

28

Lawn [41] and Chantikul et al.[40] methods. The results show that the toughness ($K_{Ic}$) of the laminates as measured using this large crack technique is more than 3 times higher than that of monolithic alumina.

Table 3-1   Specimen Designation, Hardness, and Flexure Strength** of Alumina and Composites.

| Sample Designation | Thickness (Ni, μm) | Thickness (Al₂O₃,μm) | Thickness* (Al₂O₃,μm) | Width of Sample,mm | Strength (MPa) | Hardness (GPa) |
|---|---|---|---|---|---|---|
| Ni(125) | 125 | 300 | 220 | 3.0 | 766±29 | 18.6± 0.9 |
| Ni(180) | 180 | 300 | 220 | 2.4 | 732±22 | 18.1± 0.6 |
| Ni(240) | 240 | 300 | 220 | 2.8 | 763±37 | 18.6± 0.7 |
| Al₂O₃ | | 2200 | | 2.7 | 556±45 | 18.2± 0.6 |

\*    The thickness of outer alumina layers

\*\*   All the values listed above are mean values from three of each set.
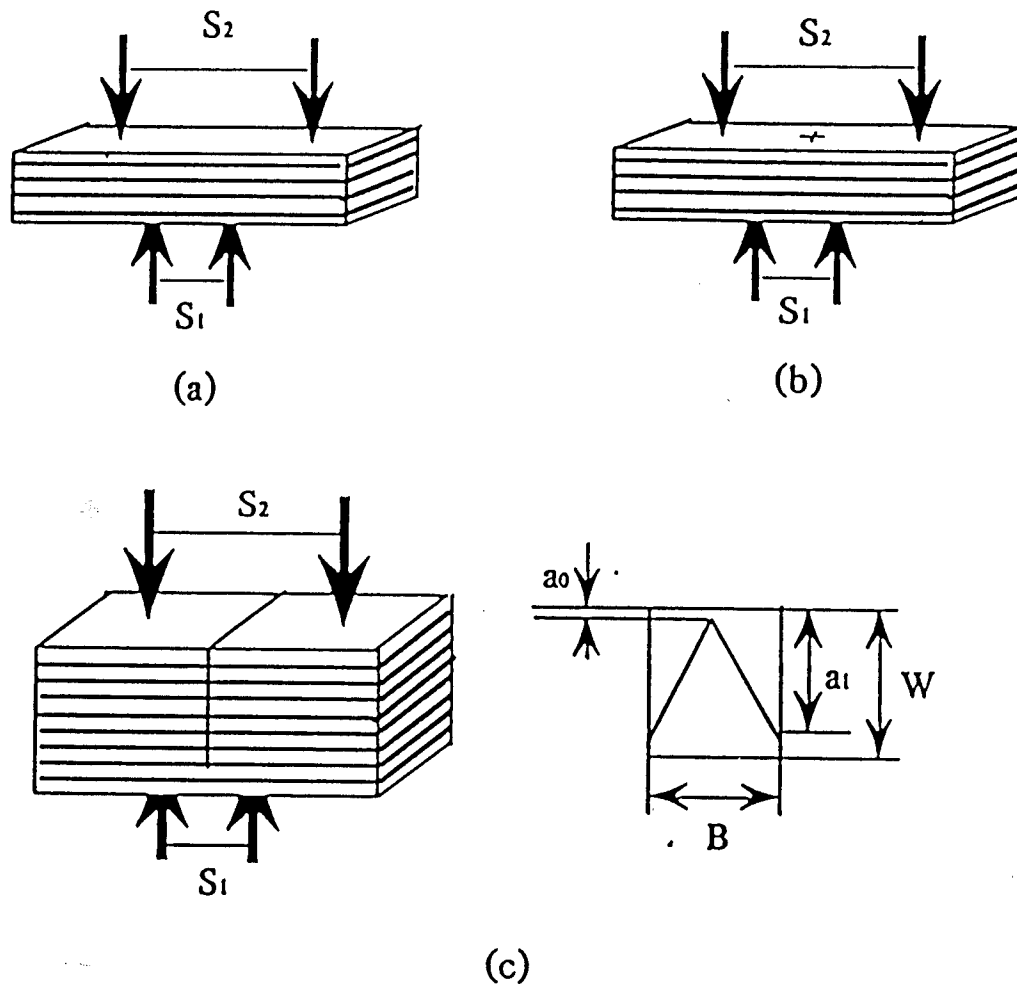
\*\*\*  ± Indicate standard deviation.

**Fig. 3-2** Schematic illustrating specimens used for flexural tests. (a) no initial crack, (b) with initial crack and (c) with chevron notch.
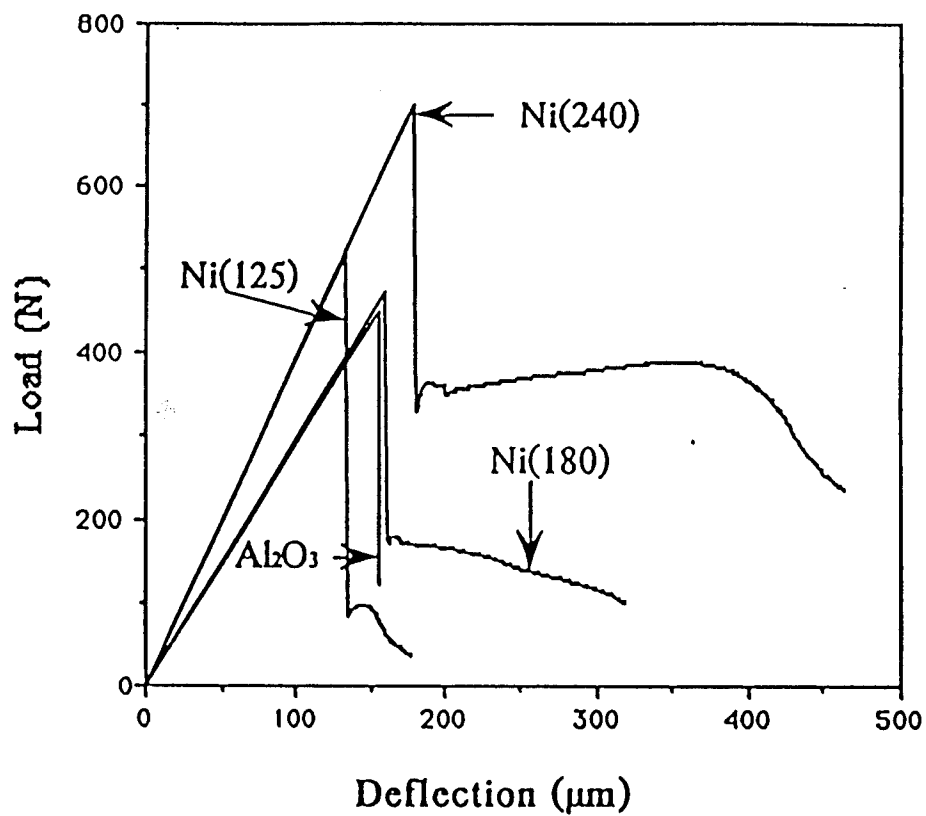
Fig. 3-3 Load-deflection curves measured for flexure strength of laminates with different thickness of nickel layers and composion with that of monolithic alumina. Designation refers to thickness as shown in Table 3-1.

32

(Λ)
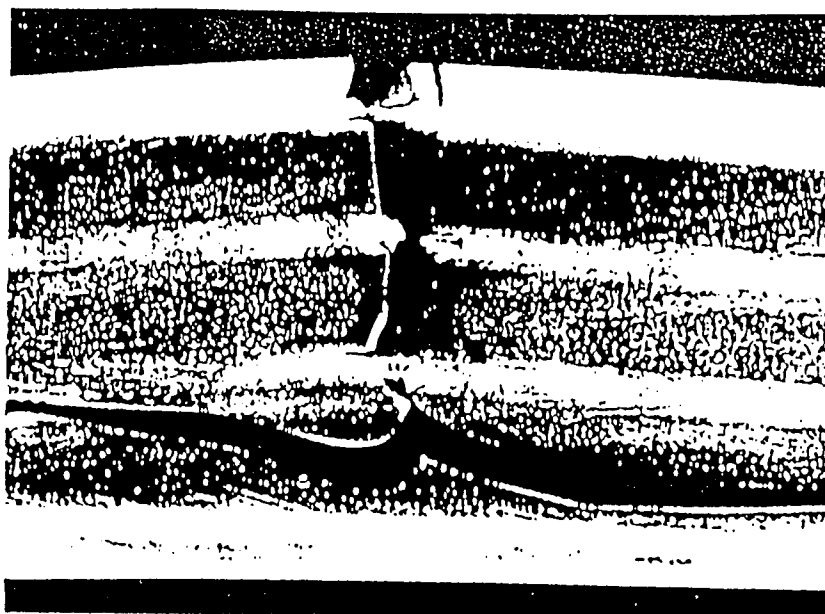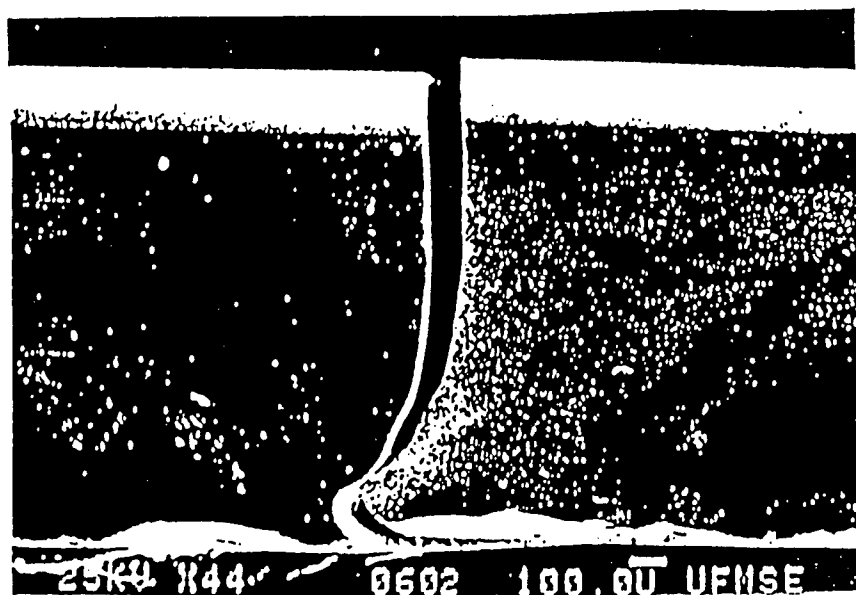


(B)

Fig. 3-4 Typical ductile bridging in laminates (Λ). The ductile layer shows plastic
behavior evidenced by necking. Local debonding also can be seen. A fractured
monolithic alumina specimen is shown (B) for comparison.

33

**Fig. 3-5** Ductile ridge marks and dimples show evidence for plastic rupture in the Nickel layer.

34
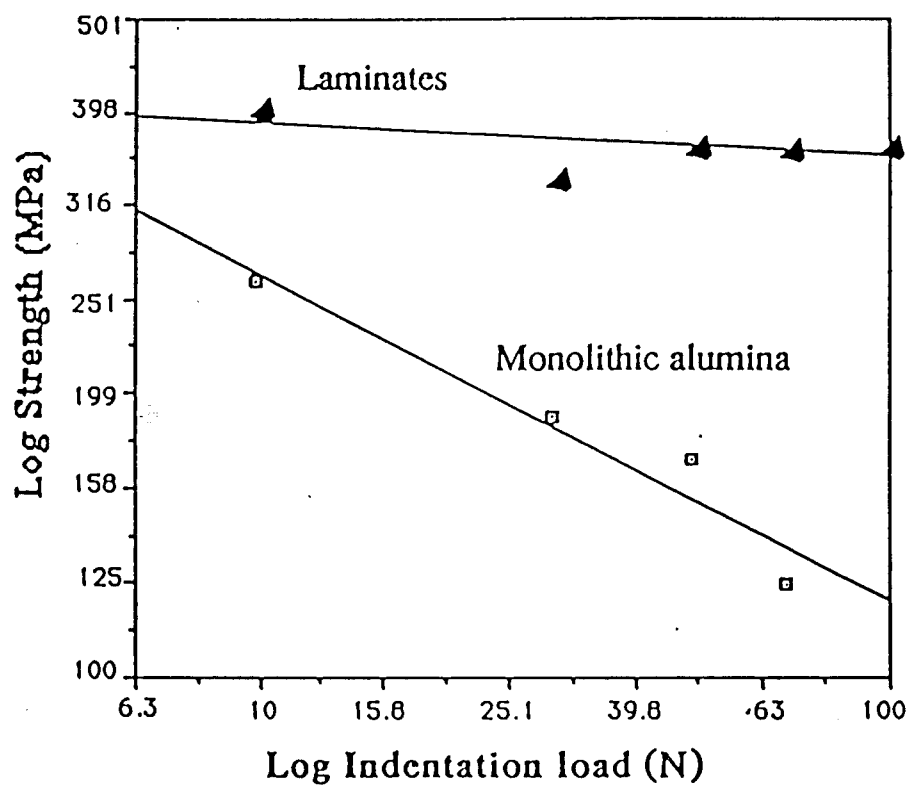
**Fig. 3-6** Log-log plots of strength versus indentation load for laminates and monolithic alumina. This figure shows that the strength of laminates are relatively insensitive to flaw size.

35
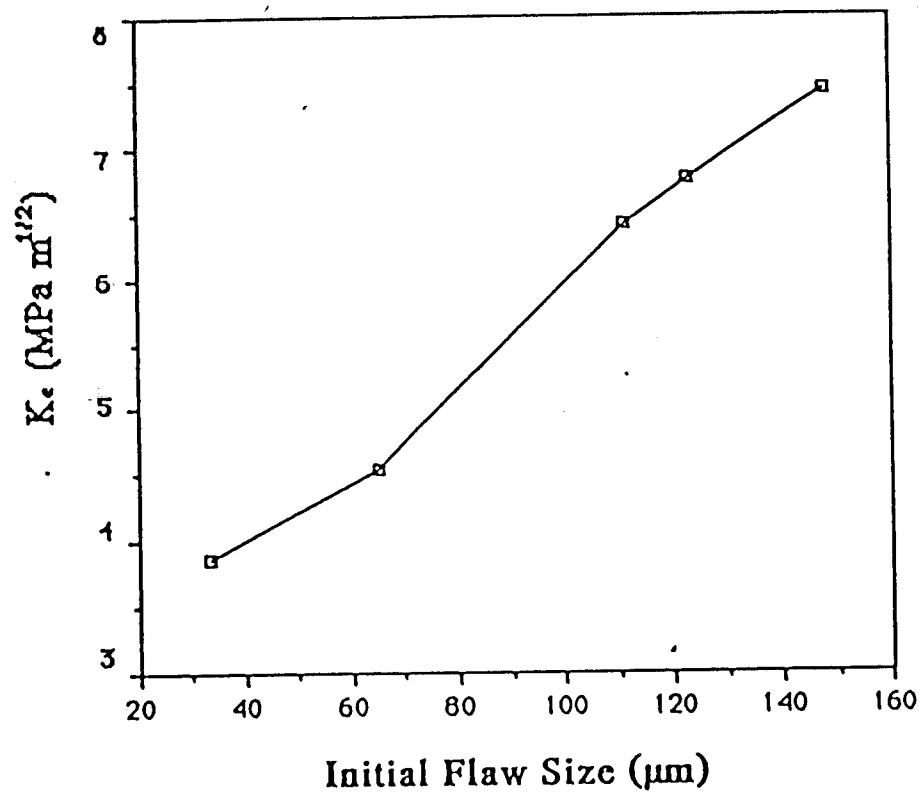
Fig. 3-7 Toughness as a function of initial crack size for Ni(180) laminated composites, "$K_{Ic}$" is calculated using Eq. (3-5). The crack size is measured from the fracture surface of as -indented bars.

Table 3-2. Toughness of Laminates.

| Sample designation | Thickness of Ni/Al$_2$O$_3$ ($\mu$m)** | Toughness (MPa m$^{1/2}$) |
|---|---|---|
| Laminates* | 180/340 | 10.7±0.4 |
| Monolithic alumina | | 2.8 ±0.4 |

\*   The laminates consist of 8 nickel layers and 9 alumina layers.

\*\*  Thickness of each nickel and alumina layer

### 3.3.3 The Effect of Residual Compression on Strength

The laminate behavior is influenced greatly by residual compressive stress in the alumina layers. This effect not only increased the flexure strength in the alumina, but also helped make the strength of the alumina layer insensitive to flaw size. An estimate of the self-equilibrating system of residual stresses which are caused by the mismatch of thermal expansion coefficients between the ceramic and metal may be calculated from the equations presented by Hsueh and Evans:[37]

$$\sigma_m = \left[ (\alpha_c - \alpha_m)\Delta T + \left( \frac{\sigma_y}{n} \right) \right] \left[ \frac{1}{E_m} + \frac{t_m}{t_c} \frac{1}{E_c} + \frac{1}{n} \right]^{-1}$$

3-6a

$$\sigma_c = -\sigma_m \frac{t_m}{t_c}$$

3-6b

where $\sigma$, $\alpha$, t, $\Delta T$ and E are residual stress, thermal coefficient, thickness of layers, cooling temperature, and Young's modulus, respectively. Subscript m and c refer to metal and ceramic, respectively. $\sigma_y$ and n are yield strength and work hardening rate of the metal. However, it is difficult to find a good experimental approach to verify these calculations. For qualitative study of the residual compression in the first alumina layer, we designed serial laminate specimens with different thicknesses of outside layers from 100 $\mu$m to 300 $\mu$m thick, and constant thickness of inside layers as for the type Ni(180) sample. Thus, stress in the alumina layer will increase with decreasing $t_c$ at fixed $t_m$ according to equation (3-6). Calculated residual compressive stresses in the outside alumina layer are 262 MPa to 146 MPa when the thickness of the outside alumina layers varies from 100 $\mu$m to 300 $\mu$m. The increase in residual compression should be reflected by the increase in flexure strength of the alumina layer. All these specimens were indented with 3 Kg Vickers diamond to create well-defined cracks in order to avoid fracture due to flaws created during processing and sample preparation. The specimens were then loaded in four-point bending at 0.078 mm/min crosshead rate. The depth of the initial crack was about 85 $\mu$m in all cases and this crack was contained in the outer layer. There is a space between the tip of crack and the interface in order to reduce the influence of the ductile layer. Fig. 3-8 shows that the flexure strength of the laminates increases with decreasing thickness of outside alumina layer in qualitative agreement with

38

eq.(3-6b). The difference in strength between the 100 $\mu$m and 300 $\mu$m layer thickness composites is 133 MPa. This result is consistent with the prediction using equation (3-6) which is 116 MPa.

The residual compression existing in the alumina layers can be demonstrated by observing the change in the length of radial cracks induced by a Vickers indenter. Vickers indentations were placed in the alumina layers. In the absence of residual stress, the length of cracks, a, around the impressions should almost be equal, due to a uniform stress field. When a residual stress field exists in the alumina layers, the length of radial cracks, a*, normal to the residual compression can be related to the magnitude of the residual stress, $\sigma_r$, by:[40]

$$\sigma_r = \frac{K_c - [\eta(E/H)^{1/2}Pa^{*-3/2}]}{\Omega a^{*1/2}}$$

(3-7)

where $\Omega$ is a coefficient related to the residual stress field ($\Omega$ = 1.128 for uniform residual stress field), and $K_c$ is assumed to be a constant. Fig. 3-9 shows radial cracks from indentation in the alumina layer of the laminates. Measured crack length, a*, which is normal to the interface is 63.2 $\mu$m. Substituting a* =63.2 $\mu$m, $K_c$ =2.8 MPam$^{1/2}$, and P =29.4 N into equation (3-8), the residual stress parallel to the interface in alumina can be determined as $\sigma_r$ = -105 MPa. This residual stress in the alumina layers suppresses crack propagation in the direction normal to the interface, which is shown in Fig. 3-9, and results in an increase in the fracture strength of alumina in the laminates. Although this latter technique is a useful qualitative technique to demonstrate the effect of residual compressive stress on crack formation, it is not expected to be quantitatively accurate because the residual stress is not actually uniform and the crack measurements are quite difficult.
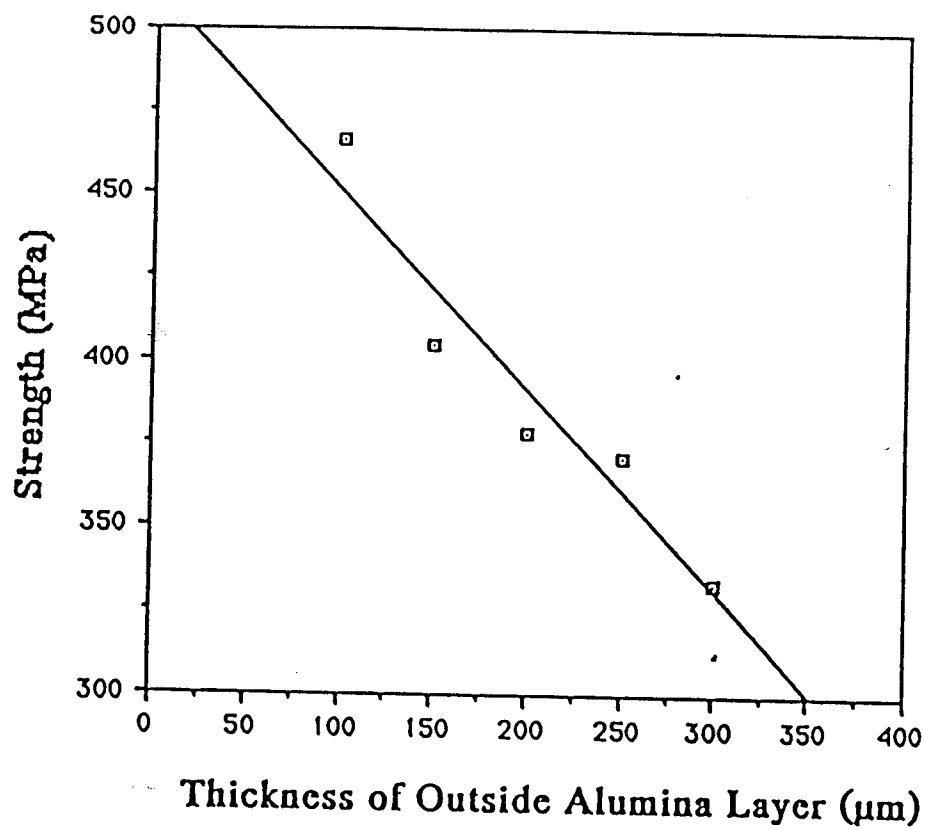
**Fig. 3-8** Indent strength as a function of the thickness of the outside alumina layer indicating the influence of residual compression in the alumina layers.

Surface
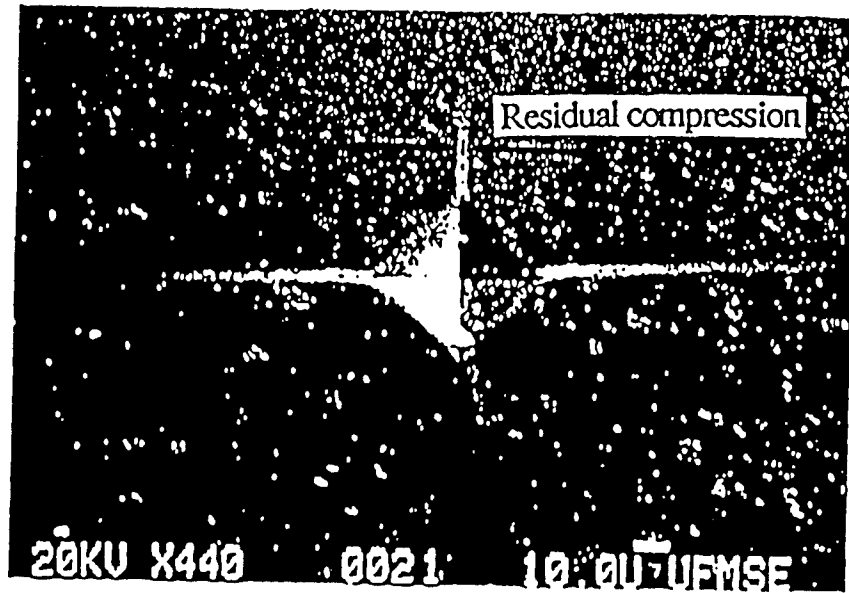


Fig. 3-9. SEM micrographs illustrating the effect of residual stress on the length of the indentation cracks in alumina layers. The arrows depict the direction of the residual compression which causes the cracks to be shorter in a direction perpendicular to the nickel layer.

41

### 3.3.4. Toughness as Measured by the Work of Fracture

When cracks initiate and propagate in the composites, they start as single cracks in the alumina layer and proceed to the metal layer. At the metal layer, the initial crack stops and restarts at another location due to metal bridging (this process will be discussed in more detail later). This process causes several cracks to propagate and leads to multiple cracking, ductile yielding in the metal and increase in the resistance to failure. Thus, the behavior initially follows the precepts of fracture mechanics, i.e., there is one crack loaded in Mode I crack propagation. Thus, we should be able to compare the initial increase in toughness by comparing $K_{Ic}$ of the monolith and of the various composites. In the case of the $K_{Ic}$ approach, the problem that arises is that the residual stress in the outer layer affects the measurement of the resistance (R) to fracture in such a way that we obtain a rising ÒR" curve. However, if we want to understand the behavior after the crack reaches the metal layer, then it is more meaningful to discuss the work of fracture or strain energy release rate. In order to understand contributions to the toughness increase in the laminates, it is necessary to study the load-displacement curves. Area under the curve divided by projected fracture surface area is the work of fracture, W. Four-point bending load-displacement curves for monolithic alumina and laminates are shown in Fig. 3-10, respectively. The curve of the laminates can be divided into two regions (Fig. 3-10): one is the elastic region (no shadow), another is the inelastic (shadowed) region. In the elastic region, the initial crack in the alumina layer has not propagated. So, the increment in elastic work, $\Delta W_e$, which compares to the area under the load-displacement curve for the monolithic alumina is attributed to residual compression in the alumina. However, in the inelastic region, since the crack is propagating, the ductile layers span the advancing crack and stretch as the crack opens until they are ruptured. The increment in the inelastic area, $\Delta W_p$, results from ductile bridging, debonding of the interface, and crack deviation, all of which were observed (e.g., Fig. 3-4). The work of fracture, W, is computed by:

$$W = \frac{1}{A} \int_0^u F(u)\,du$$

(3-8)

42

where A, F, and u are the projected fracture area, load, and displacement, respectively. Therefore, the total increment in work of fracture of the laminates, $\Delta W$, compared to monolithic alumina, is:

$$\Delta W = W^l_c + W^l_p - W^a_c - W^a_p$$

$$\text{or } \Delta W = \Delta W_c + \Delta W_p \qquad (3\text{-}9)$$

the subscripts or superscripts, e, p, l, and a, refer to elastic, inelastic, laminates, and alumina, respectively. The calculated values of work of fracture from eq.(3-8), $W^l_e$, $W^l_p$, and $W^a_e$ are 305, 1417, and 70 $J/m^2$, respectively, and the inelastic work of fracture in the monolithic alumina, $W^a_p$, is zero, using eq.(3-8). Therefore, $\Delta W_e$, $\Delta W_p$, and $\Delta W$ are 235, 1417, and 1652 $J/m^2$, respectively, [eq.(3-9)] and are the magnitudes of the respective contributions to the toughness increase in the laminate. The calculated results for different thicknesses of ductile layers are shown in Fig. 3-11. The increments in work of fracture in the elastic and inelastic regions are shown to be proportional to the thickness of the ductile layers. The residual compression increases with increasing thickness of ductile layers according to equation (3-6), such that the increment in elastic work of fracture, $\Delta W_e$, is, in turn, proportional to the residual stress. The inelastic work of fracture, $\Delta W_p$, is a major contribution to toughness of the laminates (cf. Fig.3-11).

An additional contribution to the toughness which was observed in these studies is crack renucleation. Fig. 3-12a shows that the crack started in the surface of the first layer at A and propagated toward the second layer and finally was stopped by the second layer (nickel). The crack was then renucleated beneath the second layer at B by an additional force. This point of renucleation is marked by the interruption of the load decrease on the load-displacement curve (Fig. 3-12b). The crack renucleating stress at B can be calculated using fracture surface analysis[42] and is 579 MPa ( $\sigma = K_{bl}/1.24 r_m^{1/2}$, $\sigma$ is an applied stress, the crack branching constant[42], $K_{bl} = 10.3$ MPam$^{1/2}$, and the measured radius of the mirror-mist boundary, $r_m = 206 \ \mu m$). This calculation is reasonably consistent with the result (442 MPa) computed using classic laminate plate theory. This renucleation process consumes additional energy because an additional increment of force (Fig.3-12b) is required for renucleating the crack. Thus, plastic deformation of ductile reinforcements, residual compression, and crack renucleation

caused by ductile phase crack arrest contribute to this increment in toughness of the laminates. The major contribution is governed by plastic deformation (ductile bridging associated with interface debonding and crack deviation). Furthermore, the strength insensitivity to the flaw size is attributed to a ductile layer-crack blunting mechanism and residual compressive stresses in the alumina layers. Larger cracks in the surface layer were more resistant to propagation than smaller cracks. Because of these features, the tape cast laminates appear to be good candidates for damage tolerant materials.

## 3.4 Summary

We presented studies in the manufacture and characterization of tape cast nickel/alumina multilayer composites. The strength and apparent toughness of monolithic alumina have been increased to above 700 MPa and 10 MPam$^{1/2}$, respectively, by lamination. The work of fracture in the composites Ni(125), Ni(180), and Ni(240) was 404, 1722, and 2683 J/m$^2$, respectively, as compared to 70 J/m$^2$ for monolithic alumina. It was shown that plastic deformation of ductile lamina, residual compression, and crack renucleation all contribute to toughening in these multilayer composites. No evidence was observed that cracks initiated along the interface or that failure was caused by debonding during flexure fracture. The increment of toughness of laminates has been found to be proportional to the thickness of the ductile layer. The strength of the laminates was insensitive to flaw size; this fact implies that laminates are damage tolerant and can be designed using a strength value. The role of residual stresses in the alumina layers was analyzed and discussed. However, a more precise method to characterize the residual stress in the laminates is needed.
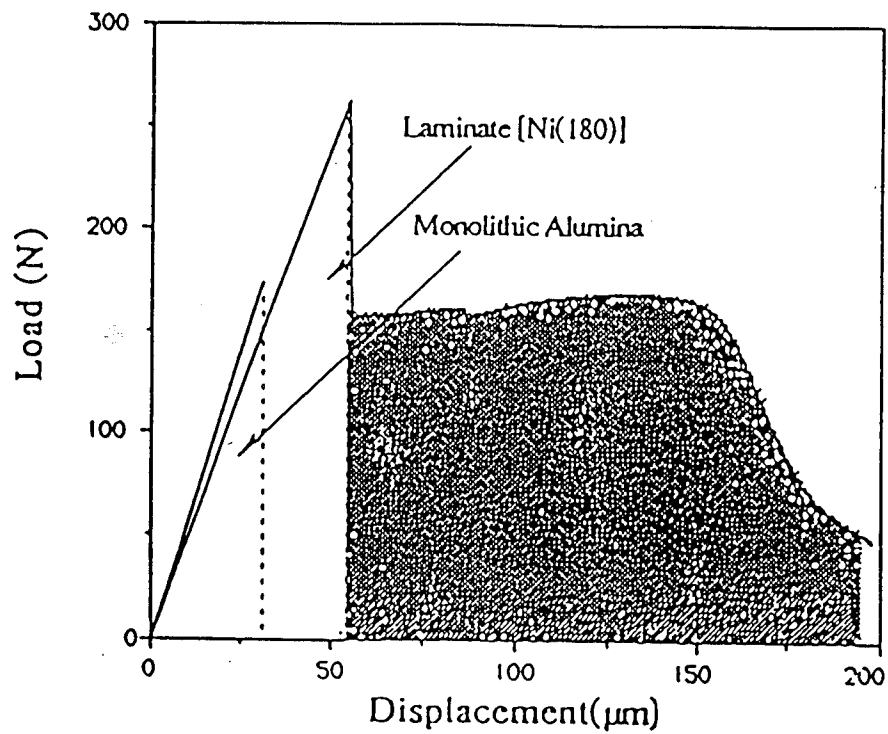
**Fig. 3-10** Difference of areas under the load-displacement curves between monolithic alumina and laminates indicates the apparent toughness increment of laminates. Shaded area designates the toughening due to inelastic processes.
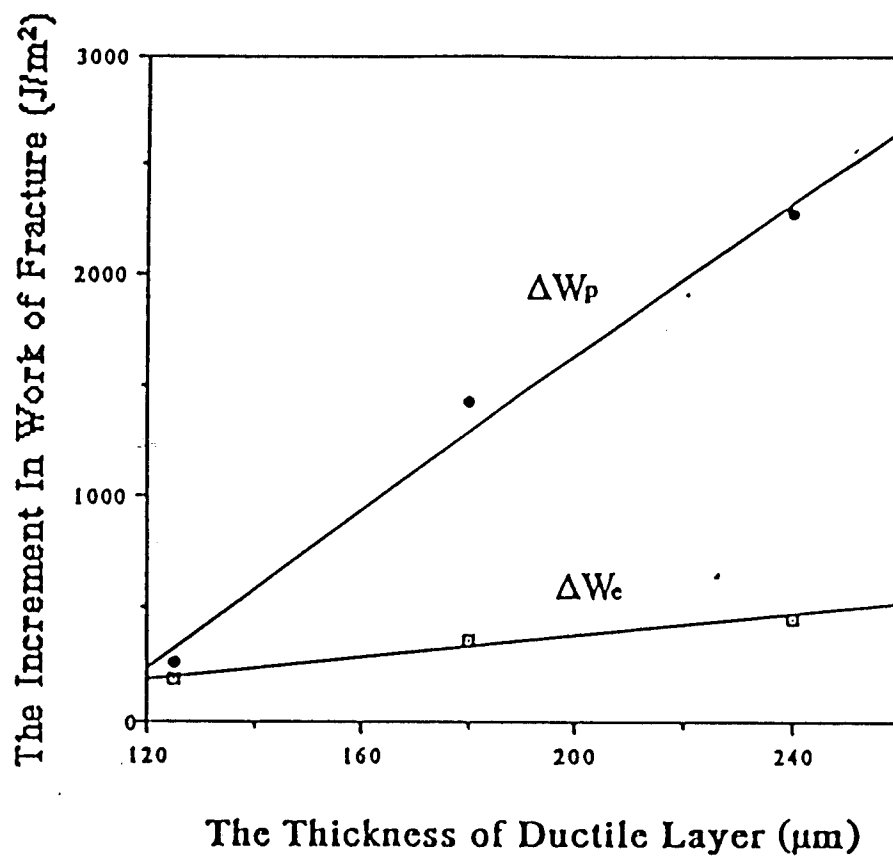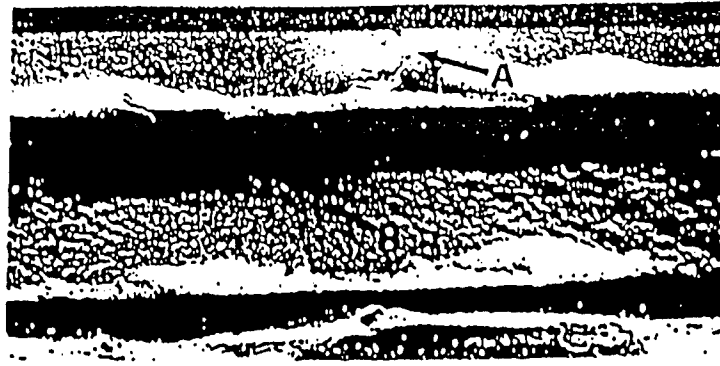
Fig. 3-11 The increments of work of fracture in the inelastic and elastic regions are proportional to the thickness of the ductile layers.

46

a. Scanning electron micrograph of the fracture surface of a laminate illustrates the crack renucleation created beneath the ductile layer at B, after fracture started at A.
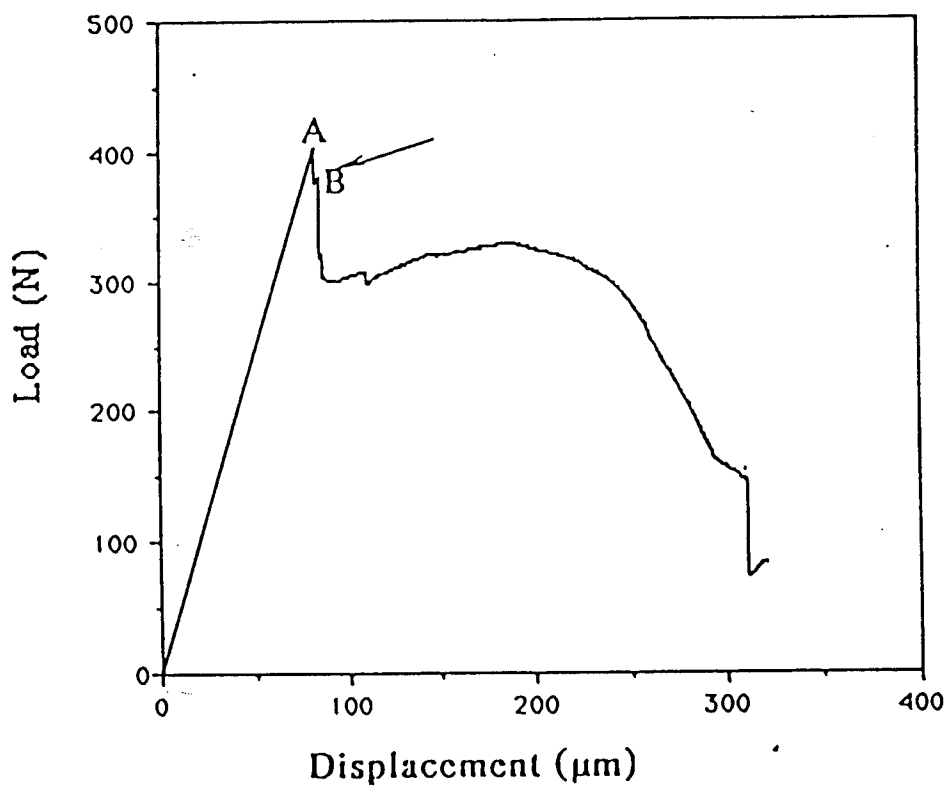


b. Load-displacement curve shows an interruption at B due to crack renucleation during load drop.

**Fig. 3-12** Scanning electron micrograph and graph illustrate crack renucleation in a laminate.

# CHAPTER 4

# CONTROL OF STRENGTH AND TOUGHNESS OF ALUMINA/NICKEL LAMINATED COMPOSITED USING INTERFACE DESIGN

## 4.1 Background about influence of interfacial conditions on plastic behavior of ductile materials

Ceramics can be toughened and strengthened by bonding ductile lamina with them[43]. The main mechanisms[22] of toughening are: Ductile layer bridging of the advancing crack and plastic deformation of the metal layers during crack propagation until they rupture and delaminate. The work of fracture which is mainly dependent on the plasticity of the ductile lamina contributes to the increment of toughness of the ceramic. The residual compressive stress which is caused by mismatch of thermal expansion in the ceramic/metal system contributes to the increment of strength of the ceramic. The amount of the increase is dependent on the specific ceramic/metal system and the bonding condition. It is important to study the plastic behavior of the ductile layers in these systems because, for most ductile materials, the plastic behavior varies with stress state.

According to the Von Mises' Criterion, the plastic yielding is related to combined stresses by[38]:

$$\sigma_o = \frac{1}{\sqrt{2}}[(\sigma_x - \sigma_y)^2 + (\sigma_y - \sigma_z)^2 + (\sigma_z - \sigma_x)^2 + 6(\tau_{xy}^2 + \tau_{yz}^2 + \tau_{zx}^2)]^{1/2} \tag{4-1}$$

where $\sigma_o$ is the plastic yield stress which is determined by the stresses, $\sigma_x$, $\sigma_y$, $\sigma_z$, $\tau_{xy}$, $\tau_{yz}$, and $\tau_{zx}$, in a Cartesian coordinate system. Therefore, the plasticity of the ductile layers which are bonded with other brittle solids in the laminated composites is different than that of ductile materials which are in an unbonded state because the bonded layers are constrained by their neighbors (high stiff brittle layers). This constrained state causes the ductile layers to be in a combined stress state rather than a uniaxial (unconstrained) state when a unixial tensile load is applied to the specimen along the nickel layer direction. Several studies showed the difference between the work of fracture and the strength of ductile materials depends on whether the ductile materials are strongly or weakly bonded with other brittle solids[44,45]. The work of fracture was calculated from the force-displacement curves in tensile tests. Features

on the fracture surface and the shape of the curves showed that the interface bonding conditions had a great influence on the behavior. Therefore, the modification of the interface is a determining factor in the strength of the interfacial bond and eventually affects the toughness and strength of laminate composites. This investigation describes experiments performed to understand the change in the work of fracture of nickel layers with the change in the profile (tortuosity) of an alumina/nickel interface. The results provide us with understanding of the toughening of ceramics using bonded ductile layers and show us how to design alumina/nickel laminated composites whose toughness and strength can be controlled by controlling the tortuosity of the interface.

## 4.2 Experimental Procedure

The nickel and alumina bond is basically a diffusion bond when it is formed in a vacuum ($<10^{-6}$ torr) or a reduced atmosphere[45]. The strength of the bond mainly depends on the atmosphere, temperature, time and pressure of processing. Once these parameters are fixed, the strength will be a function of the total contact area of metal and brittle solid components[46]. Nevertheless, the total contact area is dependent on the tortuosity of the interface. The intent of the present experiment is to modify the tortuosity of the interface by changing the total contact area of nickel and alumina layers using the same processing parameters. Thus, we can change the strength of the interface and eventually correlate this change with the variation in the work of fracture and the yield strength of the nickel layer with different interfacial tortuosity.

In order to quantitatively evaluate the tortuosity of the interface, we choose fractal profile analysis (FPA). Fractal geometry is a non-Euclidean geometry that allows for non-integer dimensions and is characterized by self-similarity and scale invariance; it has been applied to explain the topography of fracture surfaces[47]. The fractal dimension of a line resides between 1 and 2. Highly tortuous lines have larger values of the fractal dimension and smooth lines have values close to 1. The fractal dimension of the interface can be described using the Richardson equation:

$$L = KR^{1-D} \qquad (4\text{-}2)$$

where L is the measured interface length, R is the "ruler" (scale) used to measure that length,

D is the fractal dimension of the interface, and K is a constant. As the size of the ruler decreases, the total length increases. If the curve is fractal, a graph of the log length versus log ruler yields a straight line whose slope is equal to 1-D. In this way, the fractal dimension of the interface can be determined.

Very fine alumina powder (less than 1 $\mu$m in diameter) and nickel powder (around 5 $\mu$m in diameter) were cast separately into about 70 $\mu$m thick tapes using a tape casting technique by mixing them with polyvinyl alcohol based binder. It is relatively easy to experimentally achieve different fractal dimensions (tortuosity) of the interface between the nickel and alumina layers by adjusting the constitution of the tapes. The tapes were punched out in 50 mm diameter circles and then stacked together. The densified sandwich-like plates (Fig. 4-1) were produced through lamination, binder burnout, and hot pressing at 1350° C in a reduced atmosphere. All the plates were fabricated under the same processing parameters. Three type of interfacial bonds (Fig. 4-2) were used in this study: high tortuosity, medium tortuosity, and low tortuosity. All the interfaces were examined using electron microprobe analysis (EMA). In figure 4-2 we see that all have the same type of composition diffusion profiles and the same depth of diffusion. No reaction layer was observed in any case. Therefore, the only change in modification of the interface is the physical change in the interface tortuosity. These interfaces are quantitatively described in terms of the fractal dimension using the FPA approach and are listed in Table 4-1.

Tensile test specimens cut from plates which consisted of a nickel layer diffusion bonded to two alumina layers with different D values were made to measure the work of fracture of the nickel layer and are shown in figure 4-3 and table 4-1. The specimens were notched on either side of the nickel layer with a 0.5 mm thick diamond saw. Consequently, sharp cracks (Fig. 4-3) were initiated and extended from the notch roots to the interfaces by very slow tensile loading of the specimens which were mounted in a tensile test machine. All the specimens were checked afterwards to make sure only a single sharp crack was produced between the notch root and the interface. The specimens were loaded under tension in a tensile test machine at a rate of 0.0085 mm/sec. The direction of applied force was parallel to the nickel layer as shown in Fig. 4-3. The load-displacement response was recorded.
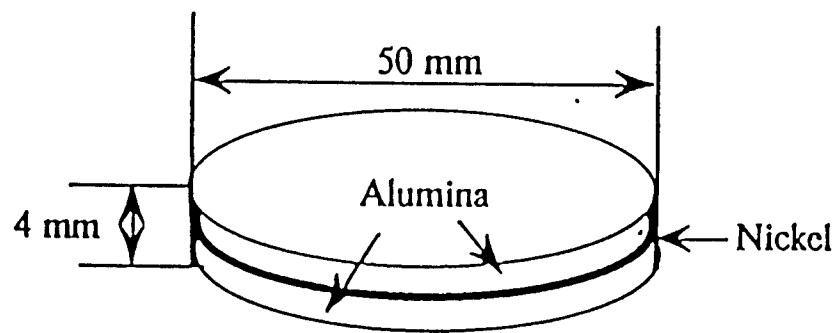
**Fig. 4-1** Schematic of the sandwich plate configuration used in the model experiments.

Table 4-1 Tensile Specimen Designation, Interfacial Fractal Dimension, Bonding Factor, Yield Strength, and Work of Fracture.

| Sample Designation | $t_o$ (mm) | D | B | $\sigma_o$ (MPa) | $W_s$ (kJ/m$^2$) |
|---|---|---|---|---|---|
| SD(1.21) | .175 | 1.21 | 3.64 | 261.7 | 75.23 |
| SD(1.07) | .175 | 1.07 | 4.22 | 233.1 | 87.02 |
| SD(1.00) | .175 | 1.00 | 20.93 | 172.4 | 432.27 |
| Ni | .175 | - | - | 118 | 601.54 |

* Ni is designated for an unconstrained nickel sheet.

## 4.3 Results and Discussion about Plastic Behavior of Single Ductile Layer Bonded by Two Brittle Layers

All single nickel layer specimens were tested in tension. The work of fracture for each sample was calculated and the results are listed in Table 4-1. The value of the work of fracture decreases with increasing value of D. Figure 4-4 shows four stress-displacement curves which are representative of each bonding case and free constrained nickel from many curves obtained in the tests, and illustrates how the shape of the curves change with D. The difference in the work of fracture of constrained nickel layers (especially for D=1.21, and 1.07) and the unconstrained nickel layer is obvious from the area under the stress-displacement curve. These differences illustrate that plastic behavior of the ductile layers can be controlled by modifying the interfacial bond (the physical change of fractal dimension, D, of the interfacial profile).

Debonding, plastic deformation, and necking have been observed during the fracture process, but for different bonding conditions, each process has different relative contributions dependant on the interface tortuosity (D). A high tortuosity (high D) results in a strong bond between $Ni/Al_2O_3$. The high stiffness of the alumina layers highly constrains the plastic deformation of the ductile nickel layers. The relatively small amount of plastic deformation is attributed to the limited amount of debonding at the interface. However, the lower D value corresponds to a weaker bond of $Ni/Al_2O_3$ which causes a relatively larger debonding length to free some of the constraint in the nickel layer from the highly stiff alumina layers during the tensile loading. This behavior results in a relatively large amount of plastic deformation of nickel which contributes to more energy absorption. Thus, the yield strength increases with increasing constraint of the ductile layers (Table 4-1). The engineering yield strength ($\sigma_0$) of the unconstrained nickel layer was computed from the load-displacement graph to be 118 MPa. Figure 4-5 shows features on the fracture surface which change from total "in plane ridges" (A), partial "in plane ridges" and partial dimples (B), and to total (tensile) dimples (C) as the nickel layer changes from a highly bonded state to an unbonded state, respectively.

The change in fracture features is evidence to indicate that the plastic behavior of the ductile layer could be influenced by the interfacial tortuosity which we can characterize in

terms of the fractal dimension D. We can normalize the work of fracture, $W_s$, by:

$$B = \frac{W_s}{\sigma_o t_o}$$

(4-5)

where we define B as a physical bonding factor which is dimensionless, $\sigma_o$ is the yield strength of the ductile layer, and $t_o$ is the thickness of the nickel layer. Since, in general, D decreases as $W_s$ increases (Table 4-1 and Fig. 4-4), then B increases as D decreases. Thus, the B value can better represent the influence of the plasticity of the ductile layer as well as the interfacial D values. To predict the amount of incremental toughening capacity, $\Delta G_c$, for a given ductile reinforcement in ductile phase reinforced ceramic composites (laminate composites) from the work of fracture Ws of the constrained single layer, we have:

$$\Delta G_c = A_f W_s$$

(4-6)

which can also be expressed as:

$$\Delta G_c = A_f B \sigma_o t_o$$

(4-7)

where $A_f$ is the area fraction of ductile layers intercepted by the crack. From equation (4-7) we see that the toughness increment, $\Delta G_c$, is a function of B for constant values of $t_o$ and $A_f$. This relationship indicates that the toughness of the composites can be controlled by controlling the interfacial tortuosity as characterized by the fractal dimension, D.
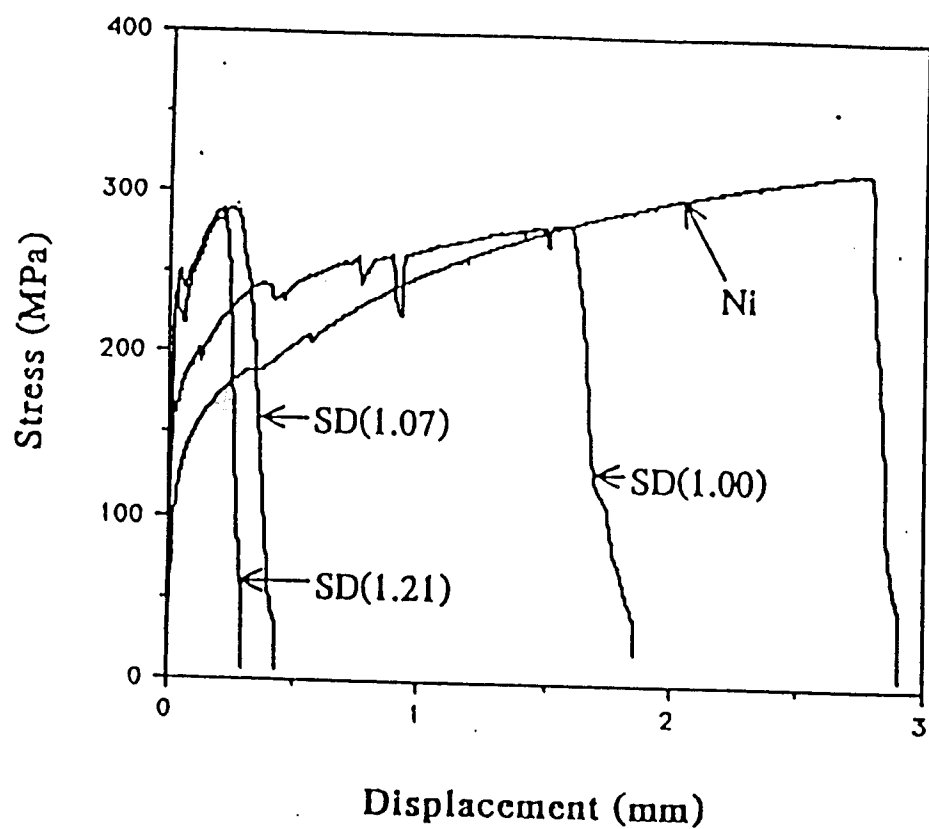
**Fig. 4-4** Stress/displacement curves for single Ni layer tensile specimens with different values of the interfacial D compared to an unconstrained nickel sheet. SD indicates the value of the fractal dimension.
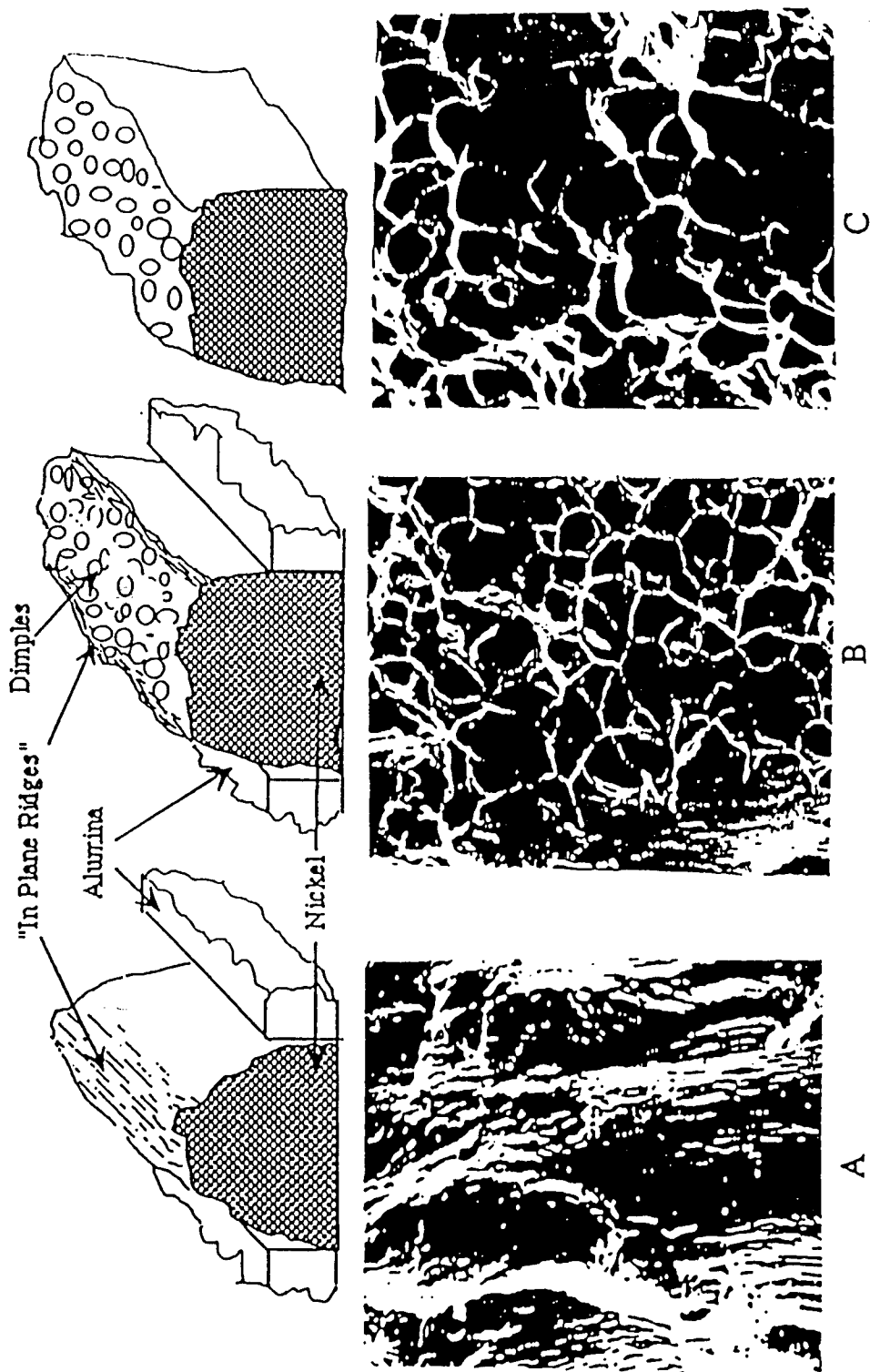
Fig. 4-5. Schematic and SEM pictures show the changes of the features of fracture surface from total "in plane ridges" (A), partial dimples and partial "in plane ridges" on the side(B), to total tensile dimples (C) as the nickel sheet changes from a highly bonded state to an unbonded state.

59

Table 4-2  Laminate Specimen Designation, Interfacial Fractal Dimension, Flexural Strength, and Work of Fracture for Laminate Composites and Monolithic Alumina.

| Sample Designation | $t_o$ (mm) | $t_{Al_2O_3}$ (mm) | D | Strength (MPa) | $W_c$ (kJ/m$^2$) |
|---|---|---|---|---|---|
| CD(1.21) | 0.15 | 0.46 | 1.21 | 267.1 | 1.69 |
| CD(1.07) | 0.15 | 0.46 | 1.07 | 190.7 | 2.04 |
| CD(1.00) | 0.15 | 0.46 | 1.00 | 157.6 | 9.16 |
| Alumina | - | - | - | 71.9 | 0.07 |

* $t_o$ and $t_{Al_2O_3}$ are the thicknesses of the nickel and alumina layers, respectively, the thickness of the outer alumina layers is about half of $t_{Al_2O_3}$.

60

## 4.4 Application of Single layer results to Laminated Composites

A previous paper[43] described that the fracture strength and toughness of alumina were increased by lamination with nickel layers placed at strategic locations. The present studies show that a change in the interface tortuosity results in a change in the work of fracture and yield strength of the nickel. We used the combined results and designed three type of laminate composites which had three different values of the interfacial tortuosity ( D=1.21, 1.06, and 1.00).

The composites consisted of four layers of pure nickel and five layers of alumina. Figure 4-6 and Table 4-2 show the composites and the thickness of each layer. The composites were made using the same processing procedure discussed in the "Experimental Procedure" section and in the previous paper[43]. Flexure test specimens 25 mm long, 2.4 mm thick and 3 mm wide were cut and polished down to 1 $\mu$m using diamond paste. An approximately 420 $\mu$m flaw was induced into the tension surface of a flexure specimen using a Vickers diamond indenter. The specimens were tested using four point bending with a 10 mm inner span and a 20 mm outer span at a 0.00085 mm/s crosshead rate; the load-displacement curves were recorded. The strength of the alumina layer which was calculated using classical laminated plate theory[32], and the work of fracture which was computed from equation (4-3) are shown in Table 4-2. The toughness (the work of fracture) of the laminated composites exhibited an increase with interfacial D decrease; however, the strength of the composites displayed an increase with a D increase. Figure 4-7 shows that higher interfacial D values which correspond to higher bonding strengths results in a small debonding length at the interface as compared to a large debonding length for the lower D values. The difference in the amount of displacement at the point when the composites fail is further evidence which indicates that more plastic deformation occurs in composites with a lower interfacial D value than a higher D value (Fig. 4-8). The amount of the displacement after the sudden peak load drop reflects the total plastic energy absorption during the composite fracture. In contrast to the work of fracture, the strength of the alumina layer of the composites was improved as D increased and corresponds to the increase in yield strength of the nickel layer as the D value increased. This result implies that the strength of the alumina in the composites was affected by the bonding strength which is proportional to the D value. The curves in figure 4-9 show the relationships

between the toughness (work of fracture), the strength, and the interfacial tortuosity as characterized by D of the laminate composites. The results shown in figure 4-9 provide an opportunity to control the toughness or strength of the composites by design of the interfacial tortuosity (D).

The work of fracture of the composites (W*) can be calculated from the constrained single ductile layer model using the following:

$$W^* = \Delta G_c + W_{Al2O3} \tag{4-8}$$

where $\Delta G_c$ is calculated using equation (4-7), and $W_{Al2O3}$, the work of fracture of the alumina alone, is computed using equation (4-3). The calculated values were compared to the work of fracture ($W_c$) of the composite measured directly from the load-displacement curves. Although the magnitude of the two curves (Fig. 4-10) do not agree, the trend is essentially the same within the conditions examined. Thus, most likely $W_c$ can be determined relatively easily: $W_c = W^*/k$, where k is a constant ($k \approx 10$). The reasons for differences between the curves are: first, equation (4-7) is derived based on discontinuous ductile reinforcement composites and may produce error if it is applied to continuous reinforcement composites; Second, two different loading methods were used in this investigation, tension for the single nickel layer and bending for the laminate composites. The error attributed to that difference is that there will be different contributions of the nickel layers to the plastic deformation in the tensile and flexure specimen. In the composites, each nickel layer was pulled to a different stress level and thus contributed different amounts of plastic energy during the composite fracture; in the tensile specimen the single nickel layer was pulled under uniform tension and thus, the contribution of plastic deformation was uniform. Nevertheless, the two results show the same tendency for the toughness and the strength of composites as a function of the interfacial tortuosity as characterized by the fractal dimension, D.

## 4.5 Summary

Fracture experiments on sandwich models of single nickel layer bonded between two stiff alumina layers gave an insight into how the plastic deformation of constrained nickel layers was influenced by physical change of the interfacial tortuosity. The plastic behavior was correlated to the toughening magnitude of ductile layers which are strategically located in brittle laminated composites. Consequently, control of the strength of the bond by modifying the interfacial tortuosity results in control of interfacial debonding length, and eventually causes control of the work of fracture and the strength. The results of the tensile sandwich model was used to design $Al_2O_3/Ni$ laminated composites. Deformation and fracture results of these composites show conformity to the tensile models and revealed that the toughness and the strength of the composites were a function of the interfacial tortuosity. The results found in this paper should help laminated composite designers to optimize their mechanical behavior.
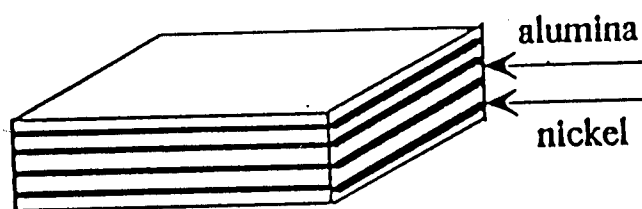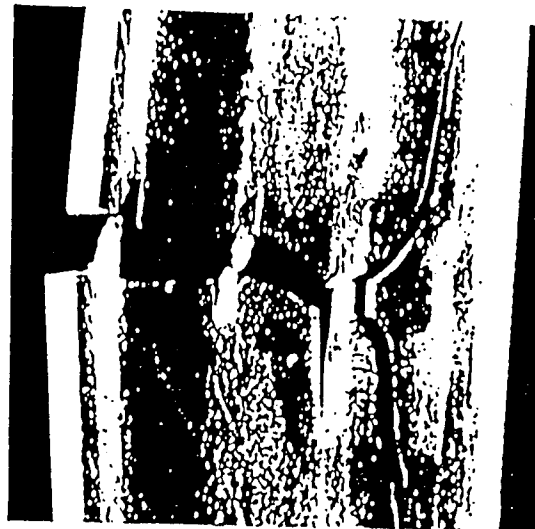
**Fig. 4-6.** A Schematic of a Nickel/ Alumina Laminated Composite.

High tortuosity (D=1.21)  Medium tortuosity (D=1.07)  Low tortuosity (D=1.00)

Fig. 4-7 SEM micrographs of Ni/Al$_2$O$_3$ laminated composites. The SEM micrographs show the change in the fracture paths due to the differences in the debonding and plastic deformation because of the different interfacial tortuosities as characterized by the fractal demension, D.
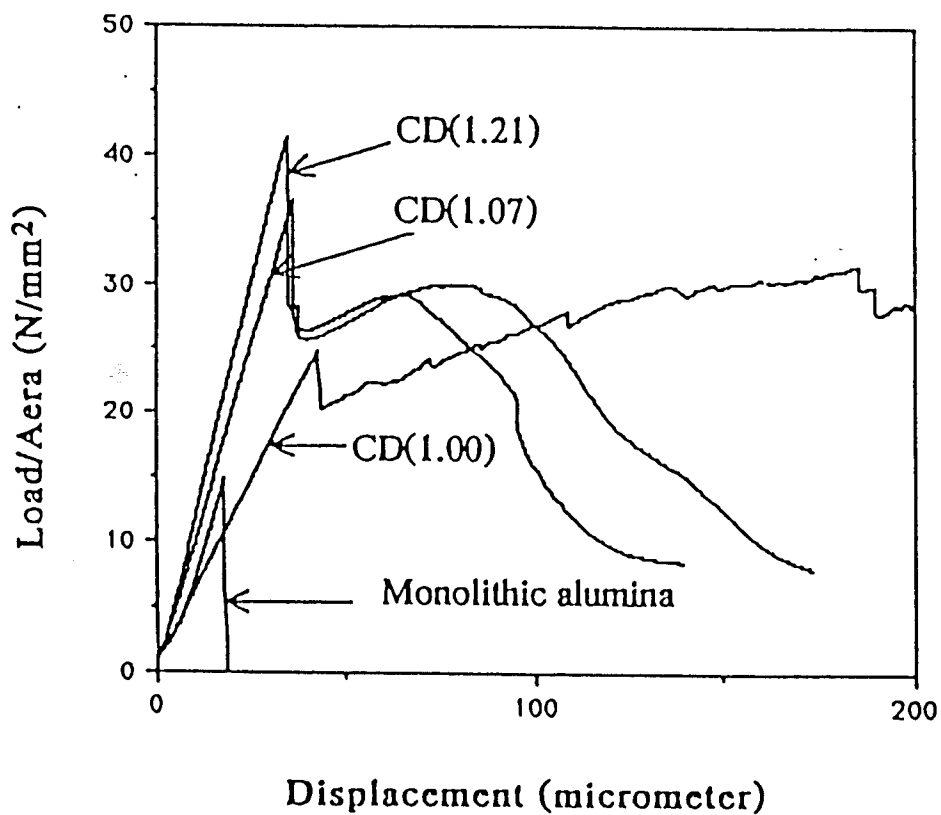
**Fig.4-8.** Load/area versus displacement curves for $Ni/Al_2O_3$ laminated composites as a function of interfacial fractal dimension, D. These curves show the increase in displacement with decrease in interfacial D values; the curve of monolithic alumina is shown for comparison.
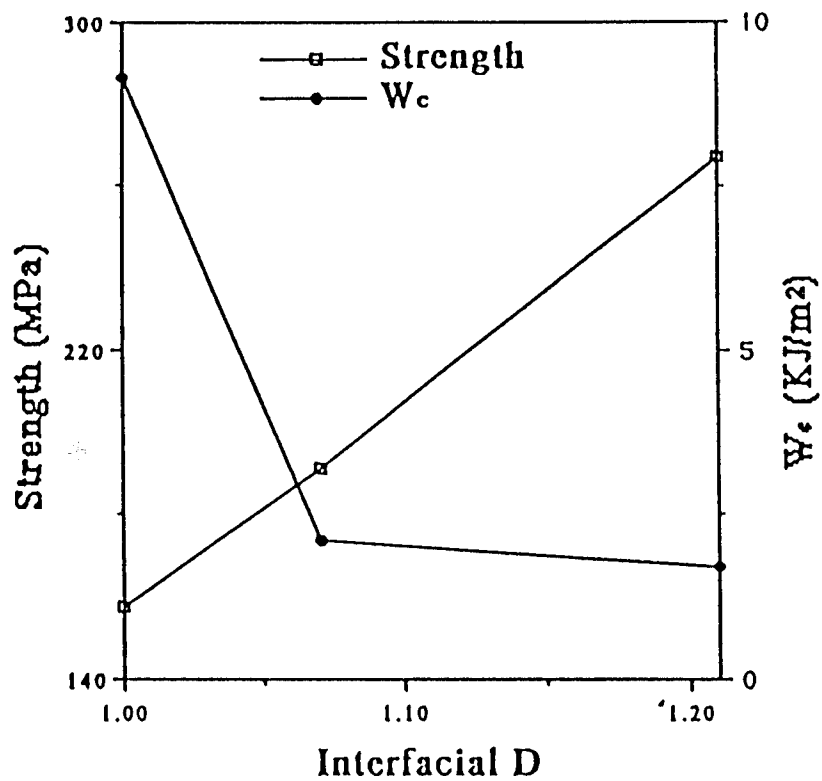
66

**Fig.4-9.** Work of fracture and strength as a function of interfacial fractal dimension, D. The curves show that the toughness increases and the strength decreases with decreasing interfacial tortuosity.
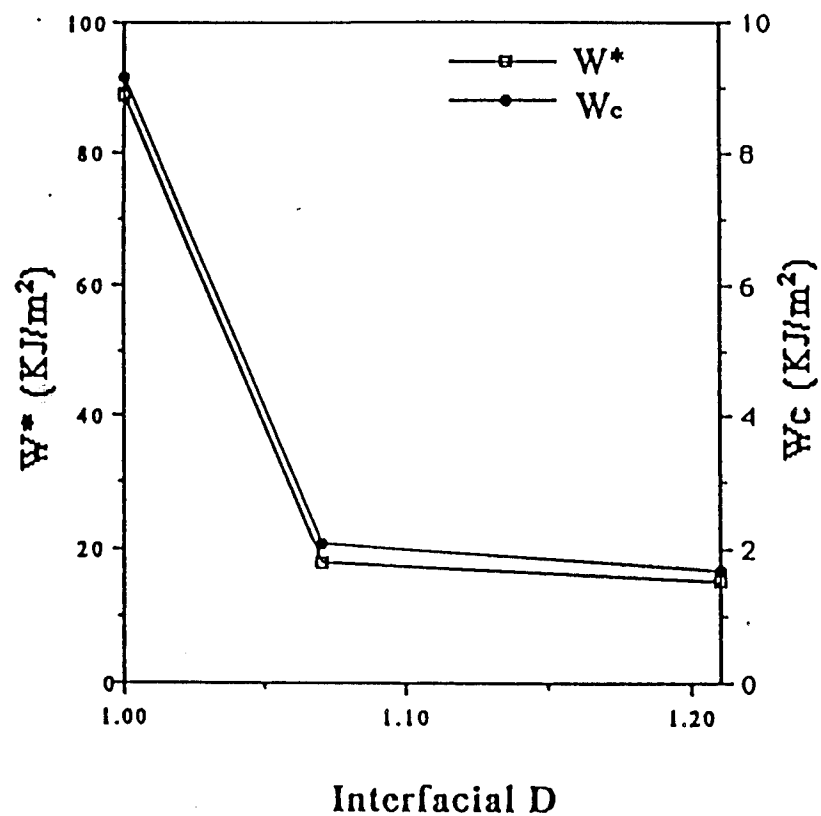
**Fig. 4-10.** Two work of fracture values, $W_c$ and $W^*$, as a function of interfacial fractal dimension, D. $W^*$ is calculated from equation 8, and $W_c$ is measured directly from the load/displacement curves, The two values show the same trend but are different in magnitude.

68

# SECTION 5

# DAMAGE TOLERANT LAMINATED COMPOSITE IN THERMAL SHOCK

## 5.1 Thermal Shock resistances of Ceramics

Alumina stands out because of the beneficial properties such as high wear/chemical resistance and high temperature retained strength, etc. However, the large statistical spread of its strength due to low toughness and low thermal shock resistance are main factors to limit its engineering applications. Many studies showed several ways to toughen alumina, e.g., second phase dispersions and phase transformation toughening[4,7]. A previous investigation[43] showed that monolithic alumina also could be toughened and strengthened due to the residual compressive stress in the alumina layers and crack blunting by ductile layers. The residual compression and crack blunting were optimized by strategic location of the nickel layers in alumina laminates. The study also showed that the strength was relatively insensitive to the flaw size. Since most applications invariably involve rapid environmental temperature variations and high heat transfer, it is important to investigate the thermal shock resistance of the laminated composites.

In general, fracture initiation resistance and (catastrophic) crack propagation resistance are two design principles used to select thermal shock resistant ceramics. For fracture initiation resistance, the capacity is described by:[48,49]

$$R^I = \frac{k(1-v)\sigma_t}{E\alpha}$$

$$(5-1)$$

where $R^I$ is the thermal shock resistance, $\sigma_t$, the strength, E, the elastic modulus, $v$, Poisson's ratio, k, the thermal conductivity, and $\alpha$, the linear thermal expansion coefficient. In order to achieve high resistance, high strength and thermal conductivity and relatively low elastic modulus and thermal expansion coefficient are required. When cracks are initiated during thermal shock, the resistance to catastrophic crack propagation, $R^{II}$, is evaluated by:[48,49]

$$R^{II} = \frac{EW_c}{\sigma_t^2(1-v)}$$

$$(5-2)$$

where $W_c$ is the work of fracture. For high ($R^{II}$) resistance, it is required to maximize the ratio

69

of the work of fracture and the elastic modulus over the strength. For most materials, it is difficult to satisfy these requirements to maximize both values of $R^I$ and $R^{II}$ because of contrastable requirements in these two equations. However, if the work of fracture of materials is significantly increased, i.e., if the ratio of increases even for a high value of $\sigma_t$ and a low value of E, then maximizing both resistances can be achieved. This paper investigates the thermal shock capacity of alumina/nickel laminated composites and incorporates the residual compressive stress influence of crack initiation in the alumina layers and the ductile layer crack blunting influence of crack propagation in the alumina layers after thermal shock ($\Delta T>$ critical quenching temperature difference, $\Delta Tc$, of monolithic alumina).

## 5.2 Thermal Shock Testing Experimental Procedure

Thermal shock experiments were performed by measuring the retained bending indent strength after quenching specimens from successively higher temperatures into water at 28 °C. An indentation technique was used to induce controlled cracks before quenching in order to control the fracture of quenched specimens. This technique was used because, for most brittle ceramics, the fracture is likely to be strongly affected by the flaws created during processing and sample preparation, and reliance on this kind of strength measurements to measure thermal shock resistance, i.e. critical quenching temperature difference, $\Delta Tc$, is unlikely to be insightful. Pre-cracking of the specimen surface was performed using a 117.6 N load with a Vickers diamond indenter. Monolithic alumina and alumina/nickel laminated composite samples were prepared by tape casting followed by hot pressing. Details of the processing for the laminated composites are described elsewhere.[43]

Four-point flexure specimens with dimensions of 25 mm (length), 3 mm (width), and about 2.0 mm (thickness) (Fig. 5-1) were broken using a tensile testing machine* with spans of 20/10 mm at a cross-head rate of 0.0085 mm/sec after thermal shock ($\Delta T$ =150 to 1200 °C). The load-displacement curves were recorded. The strengths ($\sigma_t$) and indent strength of monolithic alumina and the alumina for the laminated composites were calculated using mechanics and classical laminated plate theory[32], respectively. The work of fracture of

---

* Model 1125, Instron Corp., 100 Royall Street, Canton, Massachusetts 02021.

monolithic alumina and the laminated composite specimens with 147 N Vickers indentation load was computed using:

$$W_c = \int_0^{e*} \frac{F(e)}{A} de$$

(5-3)

where F(e) is the load, e* a displacement at the point of fracture through the whole cross section, A is the projected fracture area, and e is the displacement.

## 5.3 Thermal Shock Resistant Capacity of the Composite

The strength, $\sigma_t$, and the work of fracture, $W_c$, of both monolithic alumina and the laminated composite were calculated and are listed in Table 5-1. Since the alumina layers in the laminated composite were assumed to remain the same composition and structure as the monolithic alumina, its elastic modulus (E = 380 GPa), thermal conductivity (k = 0.29 Wcm$^{-1}$/°C), and thermal expansion coefficient ($\alpha = 8.237^x 10^{-6}$ °C$^{-1}$) were assumed to be the same as those of monolithic alumina. These parameters were put into equation (5-1) and (5-2), and the resistances to thermal shock crack initiation (R$^I$) and crack propagation (R$^{II}$) were computed and are shown in Table 5-1. Both R$^I$ and R$^{II}$ for the laminated composites were significantly improved compared to those of monolithic alumina. Thus, the retained strength and the value of $\Delta T_c$ after thermal shock of the laminated composite should be increased over that of monolithic alumina.

The retained strength after thermal shock of monolithic alumina and the laminated composite were determined for a wide range of quenching temperature differences ($\Delta T$ = 150 to 1200 °C), and strength degradation curves are plotted in figure 5-2. The monolithic alumina exhibits a rapid reduction in the strength at $\Delta T_c$ =250 °C ( about 40% of the strength of non-thermal shocked alumina). This reduction implies that the cracks in alumina begin to be propagated by thermal shock at $\Delta T > \Delta T_c$. When $\Delta T$ exceeds 950 °C, the monolithic alumina cracks into several pieces and has no measurable retained strength. Its resistance to crack propagation seems to be low, and catastrophic failure occurs when the monolithic alumina specimen has a large thermal strain energy (a large $\Delta T$).

71

When nickel layers are placed in strategic locations in the alumina laminate, the alumina retained strength after thermal shock of the composite is as high as twice the monolithic alumina (Fig. 5-2). The retained strength drop of about 30% when $\Delta T$ exceeds 350 °C compares with the strength of non-thermal shock laminated composites. After that, the strength degradation progresses slowly to a $\Delta T$ of about 550 °C; thereafter, the retained strength remains almost unchanged at about 120 MPa.

Figure 5-3 shows indentation cracks on the surface of both monolithic alumina and the composite at a $\Delta T$ = 350 °C thermal shock. The radial cracks on the monolithic alumina specimen extended approximately twice as far as before thermal shock. The radial crack before thermal shock was 2c = 421 $\mu$m. Thermal shock caused its retained indent strength to drop a relatively large amount (>40%). For the laminated composite, the radial cracks did not extend and still remained the same as before thermal shock. The radial crack in the laminated composites before thermal shock was 2c = 343 $\mu$m. The indent strength of the composite seems not to be affected by the thermal shock at this $\Delta T$ level. When $\Delta T$ exceeds 350 °C, the indentation cracks on the composite start to extend. Figure 5-4 shows thermally induced radial cracks on both monolithic alumina and the composite after $\Delta T$ = 550 °C and 1200 °C thermal shock, respectively. Even though thermal cracks started to be initiated or propagating in the composite specimens, the situation seems to be much less severe compared with thermal cracks in the monolithic alumina specimens. No cracking in the composite specimens was observed even under a severe $\Delta T$ = 1200 °C thermal shock. No delamination was observed even after wide ranges of temperature differential in thermal shock. However, delamination is often observed along the interface in many ceramic/metal systems.[14,35] The behavior of the present composites indicates that a very good bond can be formed between alumina and nickel using tape casting followed by hot pressing.

Figure 5-5 shows a side view of the composite specimen which experienced a $\Delta T$ = 1200 °C thermal shock. The figure shows many cracks in the alumina layers which were caused by a large amount of thermal-strain energy. However, the ductile layers which resulted in higher $R^{II}$ values in the composite stopped catastrophic crack propagation through the cross section and the residual compressive stress left the composite with a retained strength about

120 MPa. Unlike the composite, when the thermal-strain energy reaches such a large amount in monolithic alumina, the thermally induced cracks propagate through the cross section of the samples and cause the specimen to fracture in several pieces.

The increase of resistance to thermally induced crack propagation is attributed to the nickel layer crack blunting in the composite. The high magnification SEM micrograph in Fig. 5-5b shows that a crack was blunted and arrested by the nickel layer at the interface. This picture also is evidence that a good bond between alumina and nickel still exists in the composite after the specimen had a severe thermal shock ($\Delta T = 1200$ °C). Load-displacement curves (Fig. 5-6) show a decrease in the stiffness of the composite but an increase in its plastic behavior when $\Delta T$ exceeds 350 °C. This toughening of the composite was attributed to the amount of thermally induced cracks initiated at the grain boundaries in the alumina layer and blunted at the interfaces by the nickel layers during high thermal-strain energy thermal shock.

Fracture path analysis reveals that the thermally induced cracks were blunted and arrested by ductile layers, and the ductility of nickel layers absorbed amount of fracture energy by local plastic deformation (Fig. 5-5b). The behavior of the ductile layers contributes to an increase in the amount of resistance to thermally induced crack propagation. Further study was focused on the cause of increase to resistance of thermally induced crack initiation, $R^I$, in the composite. The previous paragraph showed that the critical quenching temperature difference, $\Delta T_c$, of the composite increases above 100 °C over that of monolithic alumina. From equation (5-1), an increase in $R^I$ is attributed to an increase in the strength of the alumina, $\sigma_t$, because E, k, and $\alpha$ values of the alumina in the composite are assumed the same as those of monolithic alumina. Therefore, the increase of strength is attributed to a residual compressive stress in the alumina layers due to the thermal expansion coefficient mismatch between the alumina and nickel layers. The residual compressive stress in the alumina layers was determined using an indentation technique.

The existence of residual compression in the alumina layers can be demonstrated by observation of the change in the length of the radial cracks induced by a Vickers indenter. Vickers indentations were placed in the alumina layers. In the absence of residual stress, the

73

length of the cracks, c, emanating from the adjacent corner of the impressions should be almost equal, due to a uniform stress field. When a residual stress field exists in the alumina layers, the length of radial cracks, $c^*$, normal to the residual compression is prevented from growing and can be related to the magnitude of the residual stress, $\sigma_r$, by:[40,37]

$$\sigma_r = \frac{K_c - [\eta(E/H)^{1/2}Pc^{*-3/2}]}{\Omega c^{*1/2}}$$

(5-4)

where $\Omega$ is a coefficient related to the residual stress field ($\Omega = 2H/\pi$ for a uniform residual stress field[37]), $\eta$ is a material-independent constant for Vickers-produced radial cracks ($\eta$ =0.014 for alumina[50]), $K_c$ is a measure of the toughness ($K_c$ = 2.8 MPam$^{1/2}$)[43] H is the hardness of alumina (H = 18.2 GPa)[43], and P is the indent load. Three different indent loads were selected (19.8 N, 29.4 N, and 39.2 N) depending on the convenience for crack measurement and the avoidance of an influence by the interfaces. Figure 5-7 shows the radial cracks and Vickers impressions for these three indent loads. The residual stress was calculated using equation (5-4) and plotted versus the indent load (Fig. 5-8). The calculations result in about 110 MPa compressive residual stress existing in the alumina layers. This 110 MPa compressive stress can account for much of the over 120 MPa retained strength increase and 100 °C increase in $\Delta T_c$ for the laminated composites over the monolithic alumina, that was observed in the strength degradation curves of Fig. 5-2.

There is no evidence showing that the higher thermal conductivity of nickel contributes to the improvement in thermal shock resistance capacity of the laminated composites.

Table 5-1  Specimen Designation, Strength, Work of Fracture, Thermal Crack Initiating Resistance, and Thermal Crack Propagating Resistance.

| Sample Designation | Thickness (Ni, mm) | Thickness (Al$_2$O$_3$,mm) | Strength (MPa) | $W_c$ (KJ/m$^2$) | $R^I$ (KW) | $R^{II}$ (mm) |
|---|---|---|---|---|---|---|
| LC180 | 180 | 320 | 732±22 | 1.72 | 5.36 | 1.62 |
| Al$_2$O$_3$ | | 2000 | 556±45 | 0.07 | 3.86 | 0.12 |

* LC180 = Alumina/Nickel Laminated composite, Al$_2$O$_3$ = Monolithic Alumina.

** The thickness of outside alumina layers is about 200 μm.

75
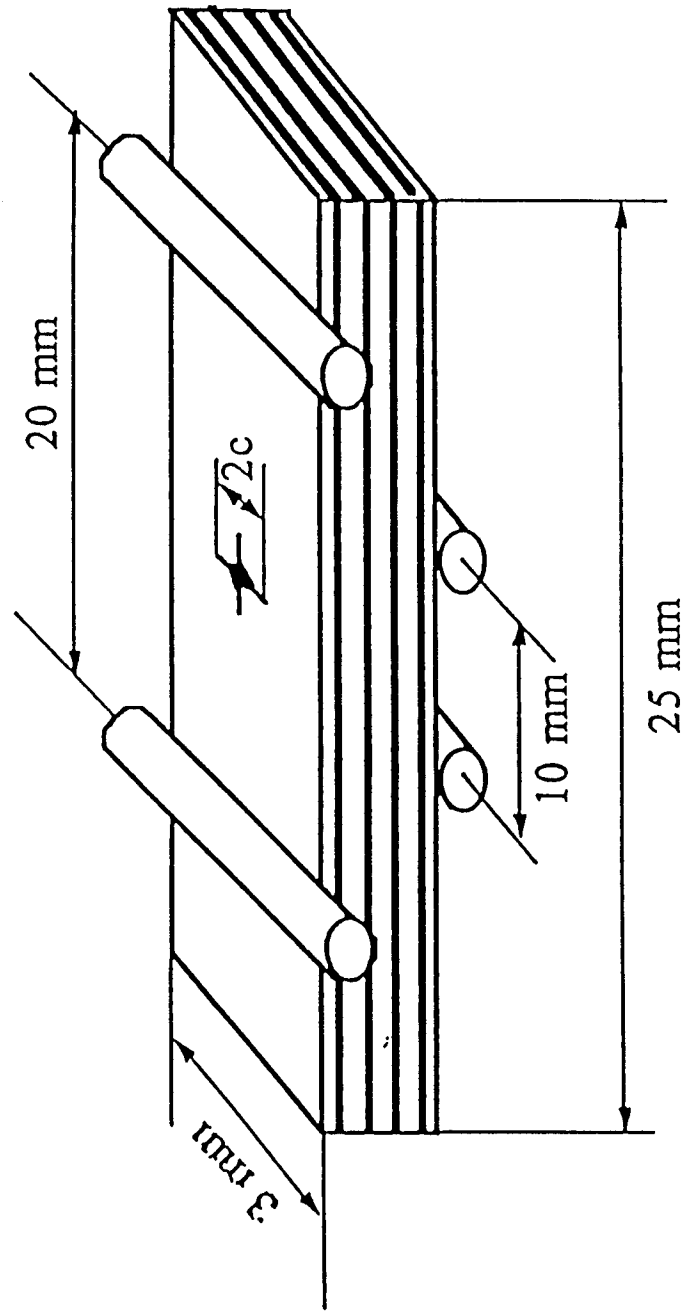
Fig. 5-1 Schematic illustrating specimen used for retained strength measurements. $2c = 421 \, \mu m$ and $343 \, \mu m$ for monolithic alumina and the laminated composite, respectively.
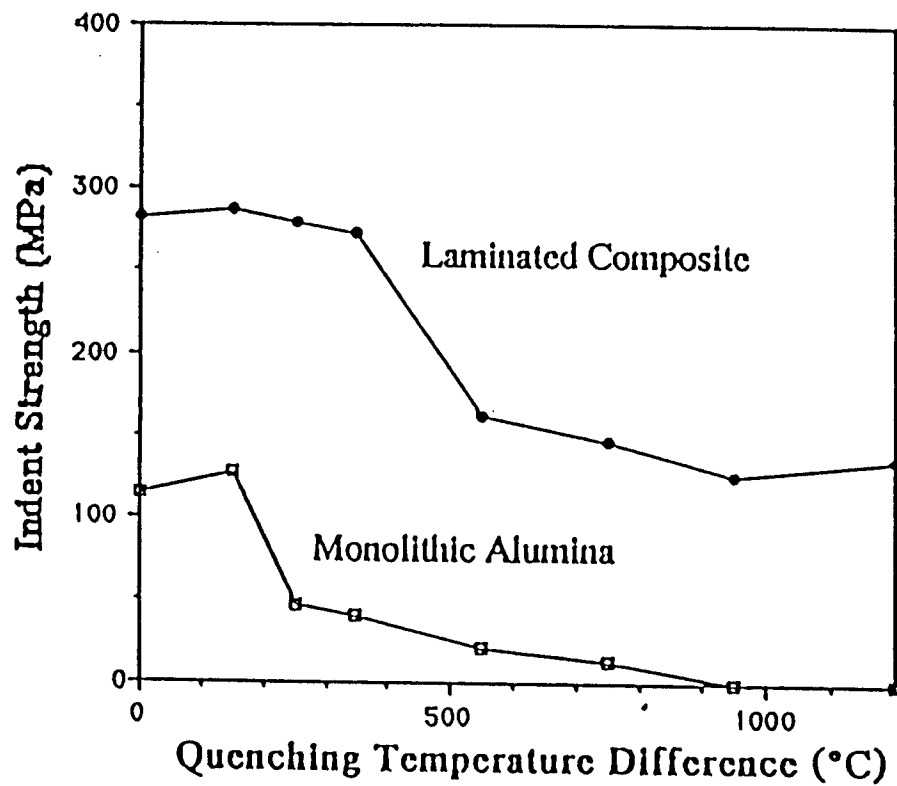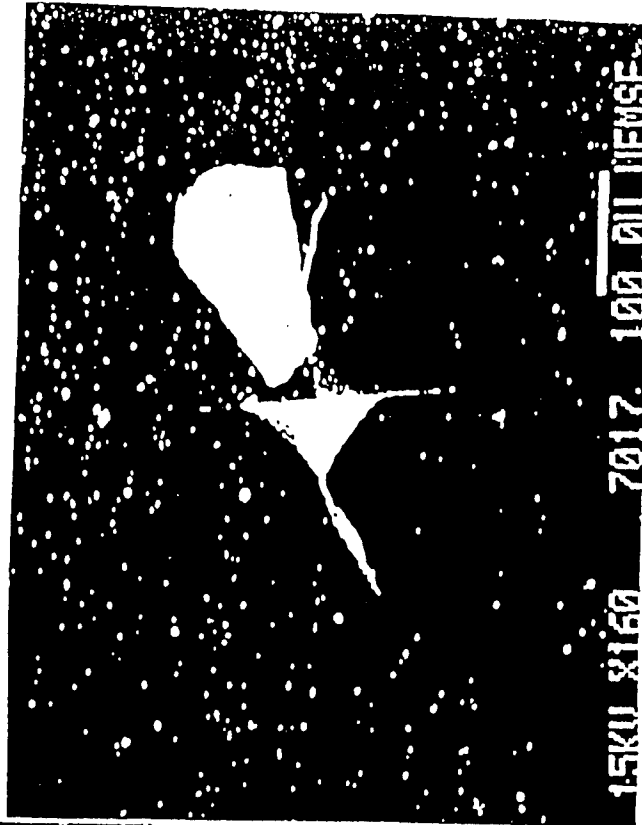
**Fig. 5-2** Strength degradation curves for wide range of quenching temperature difference thermal shock show an increase of thermal shock resistant capacity of the laminated composite over monolithic alumina.
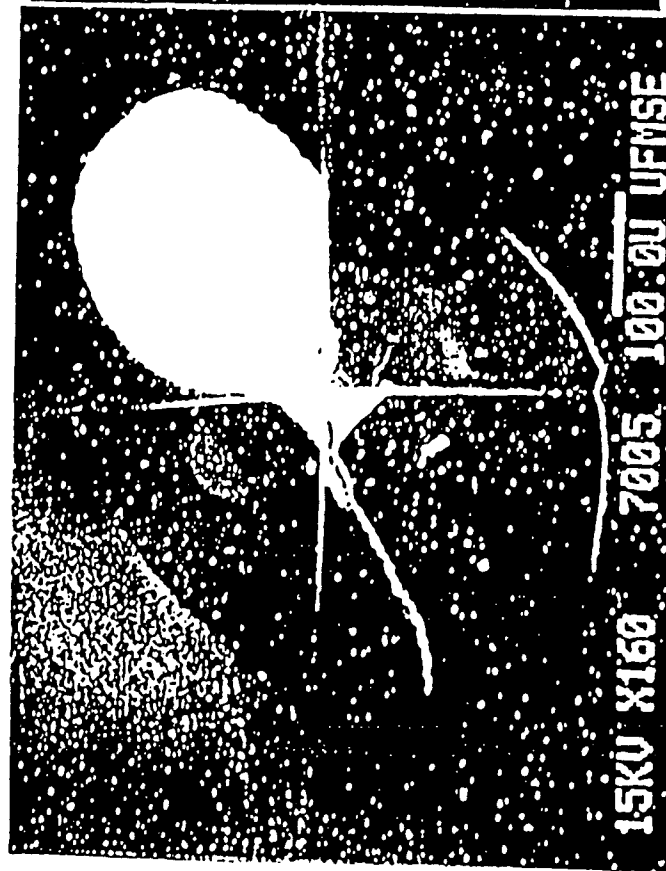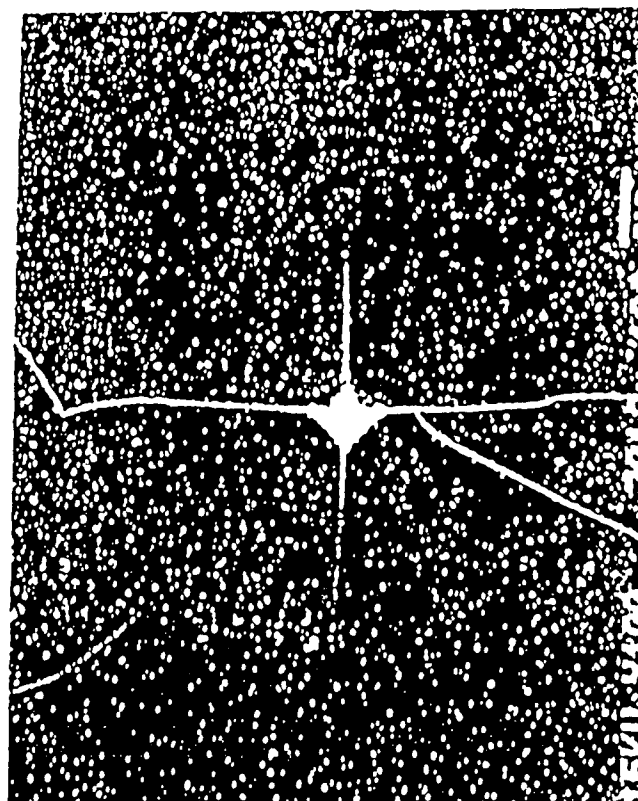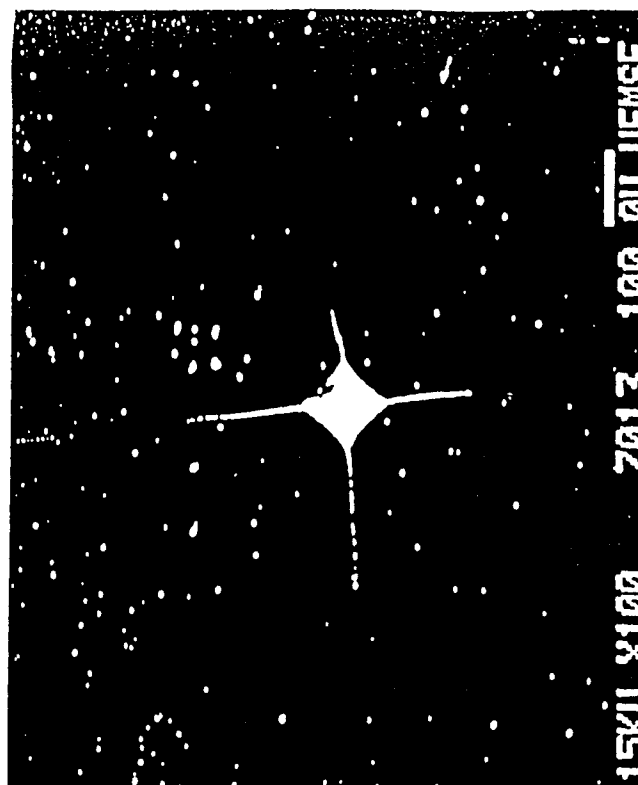
Monolithic Alumina          Laminated Composite

Fig. 5-3   SEM graphs of indentation cracks after thermal shock. Indent radial cracks on the laminated composite did not extend after a $\Delta T = 350$ °C thermal shock compared to monolithic alumina in which the cracks extended. This indicates $\Delta T_c$ of the composite increased.

Laminated Composite

Monolithic Alumina

(a)
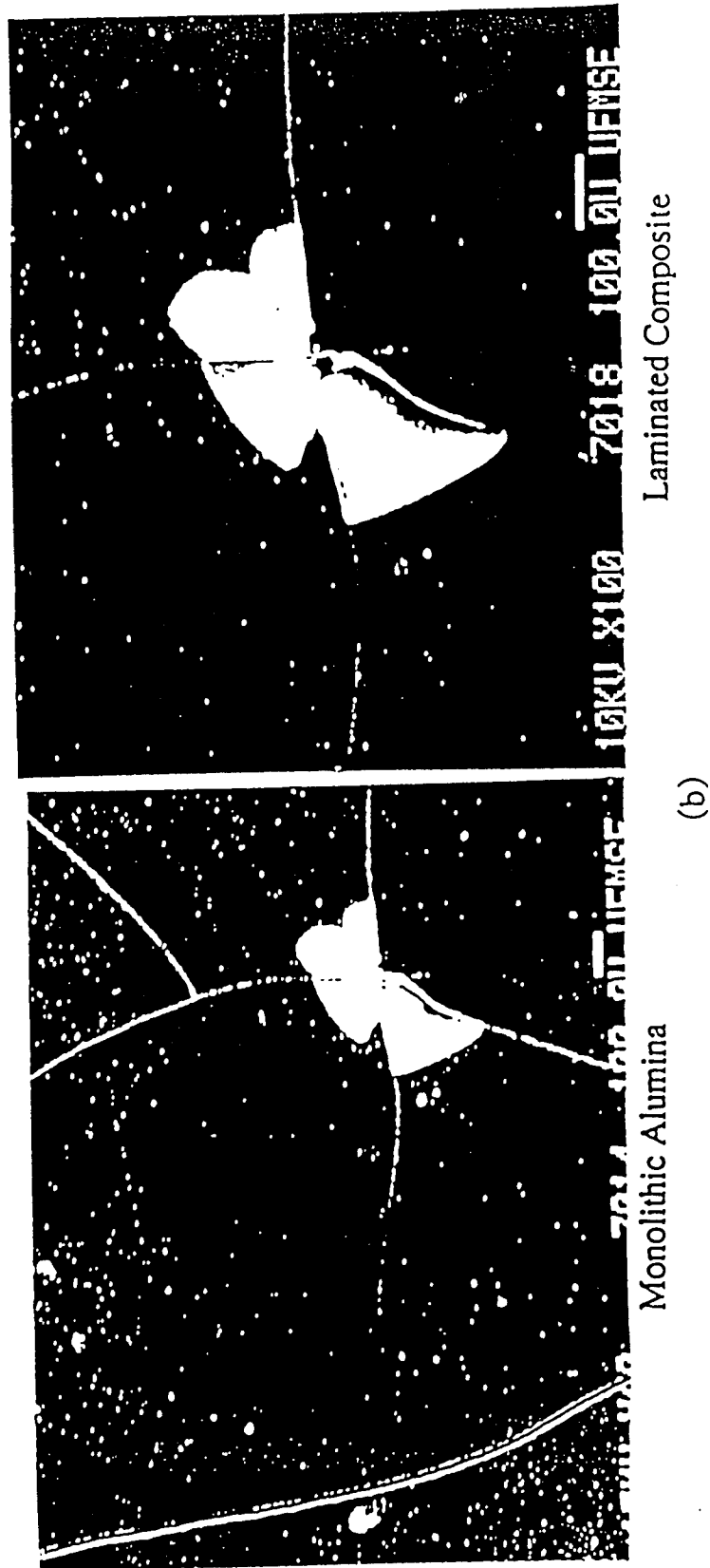
Monolithic Alumina

Laminated Composite

(b)

Fig. 5-4 SEM graphs of indentation cracks after thermal shock at (a) 550 °C and (b) 1200 °C. Less severe damage was caused by different (ΔT) thermal shock conditions in the laminated composite compared with monolithic alumina.
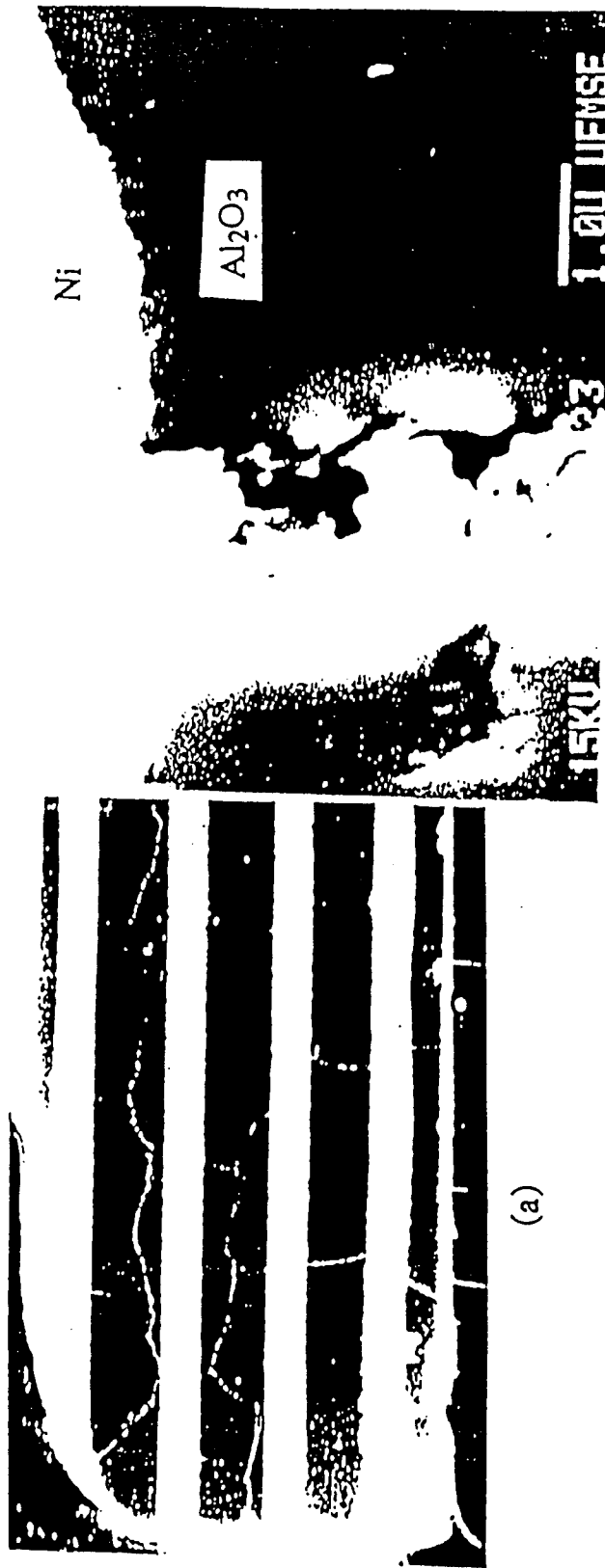
Ni

Al₂O₃

1.0U UFMSE

(b)

(a)

Fig. 5-5 (a) and (b) SEM micrographs of cracks in a laminated composite after thermal shock. Thermal cracks were stopped (blunted) by ductile layers in the laminated composite after $\Delta T = 1200$ °C thermal shock, which illustrated that high resistance of thermal crack propagation was achieved. High magnification SEM picture also shows no delamination after the severe thermal shock in (b).
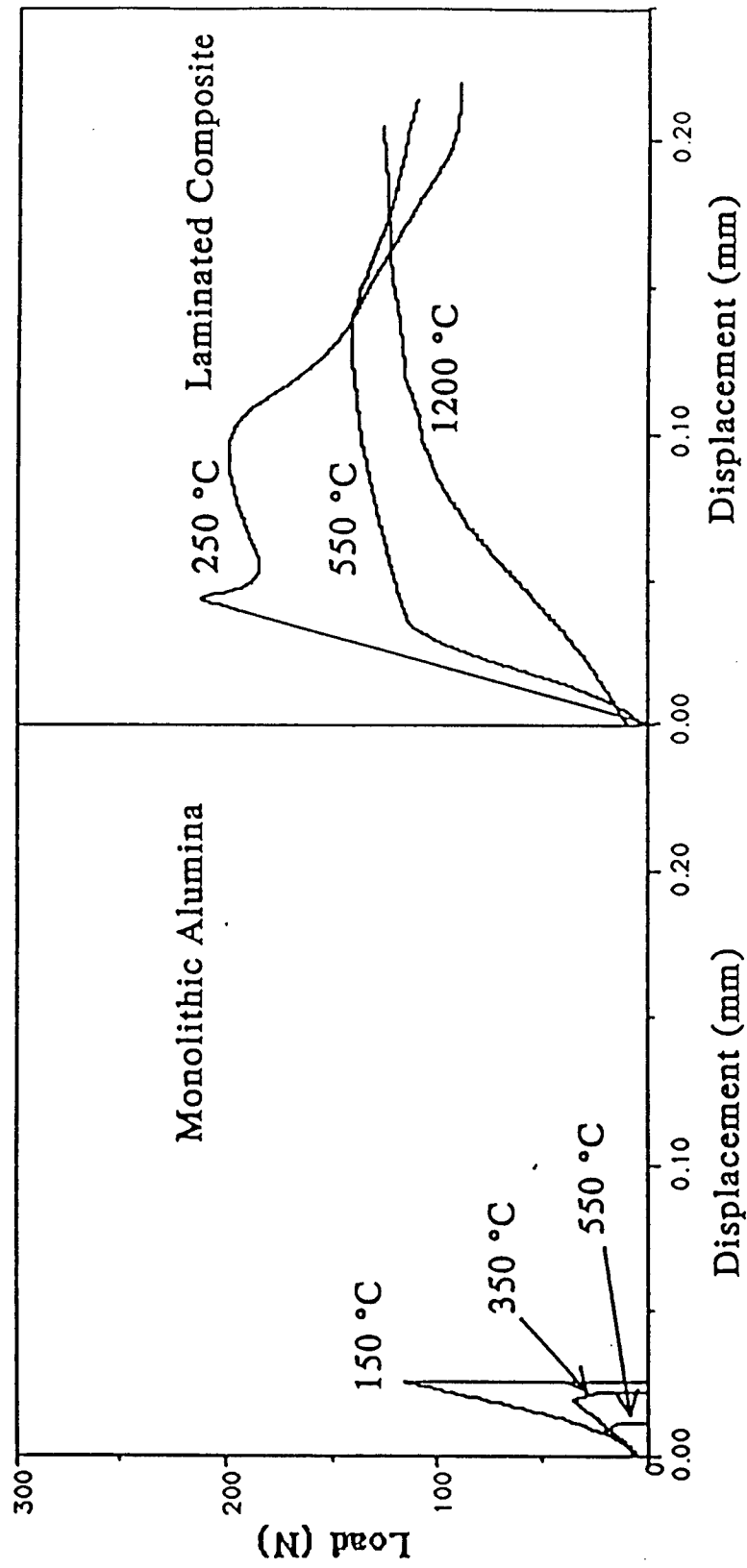
Fig. 5-6  Load-displacement curves after thermal shock of monolithic alumina and laminated composites. This figure shows that the plastic behavior of the laminate was significantly improved over monolithic alumina.
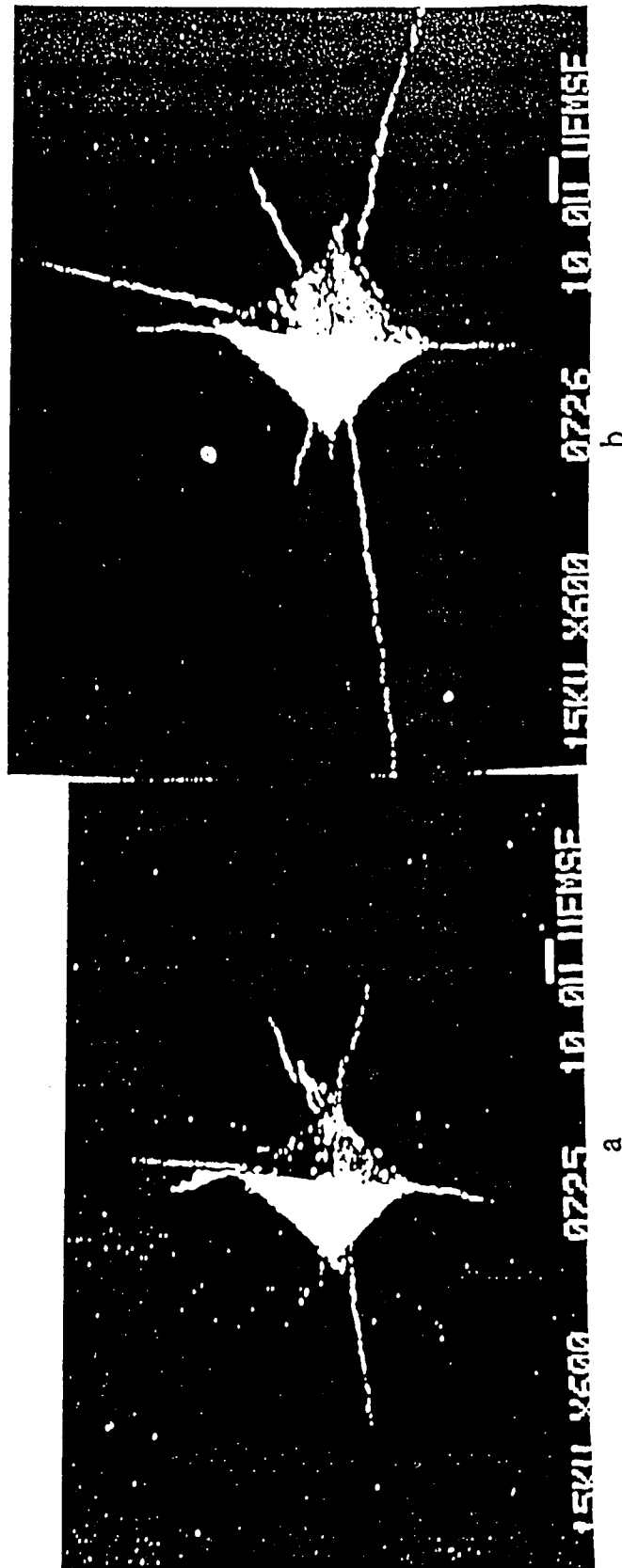
Fig. 5-7 SEM pictures of indentation cracks in the alumina layers near the alumina/nickel interface (top of figures). SEM micrographs illustrate the effect of residual stress on the length of the indentation cracks in the alumina layers. a and b show radial cracks which were initiated by 19.8 N and 29.4 N indent loads, respectively.
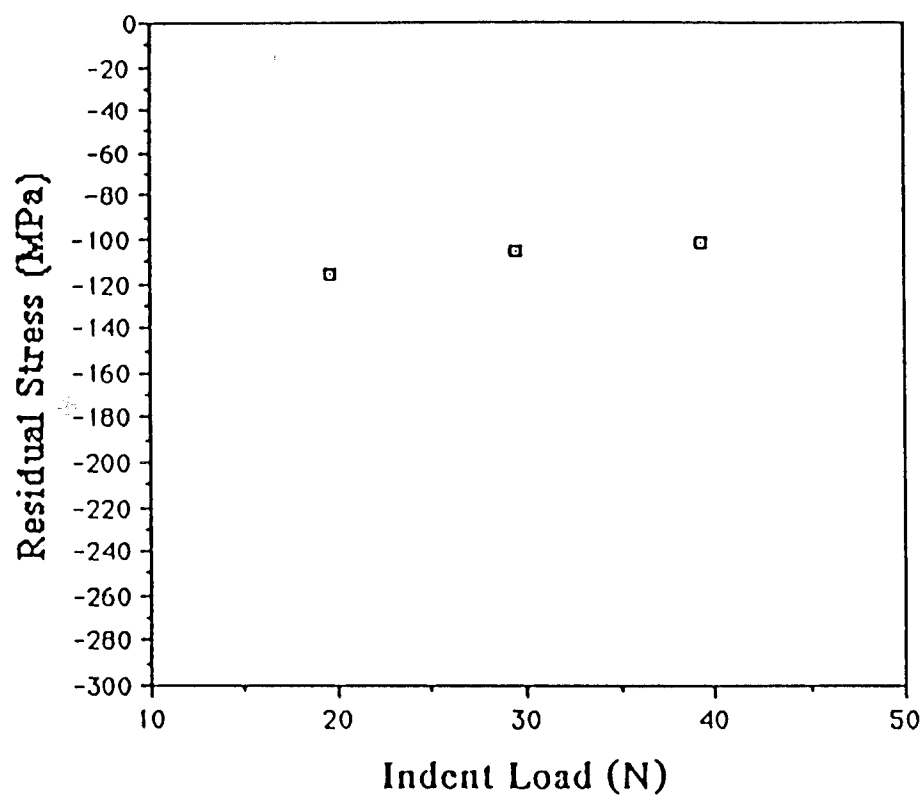
83

Fig. 5-8 Compressive residual stress versus indent load as described by eq. (5-4).

## 5.4 <u>Summary</u>

The thermal shock behavior of tape cast alumina/nickel laminated composites exhibit some attractive features. The retained strength after thermal shock for a wide range of temperatures ($\Delta T$ =150 °C to 1200 °C) was increased by more than a 120 MPa increment compared to that of monolithic alumina corresponding to each $\Delta T$. Moreover, the critical quenching temperature difference was enhanced more than 100 °C over the monolithic alumina ($\Delta T_c$ =250 °C). The non-catastrophic fracture for the laminated composite is desirable for industrial applications. This investigation found that the increase in both resistance of thermal crack initiation and crack propagation is attributed to a compressive residual stress existing in the alumina layer and crack blunting by the nickel layers. This type of laminated composite exhibits a way for improvement of thermal shock resistance and damage tolerance in ceramics.

## SECTTION 6

## CONCLUSIONS

Ceramic laminated composites were designed by inserting several (Ni) ductile layers into laminated alumina ceramic at strategic locations using tape casting and subsequent hot pressing. This design produced a residual compressive stress field in the alumina layers and arrested cracks because of the ductility of the nickel layers, and resulted in an increase in the resistance to crack initiation and propagation. This composite has a hard surface that is reasonably strong, and possesses chemical inertness and thermal stability. The mechanical behavior of the constrained nickel layer (bonded nickel layer) and the laminated composite was systematically studied. The results of the work in this study are concluded as follows:

Alumina/nickel laminated composites can be successfully fabricated using tape casting and subsequent hot pressing

The tape casting and subsequent hot pressing processes for fabrication of alumina/nickel laminated composites have been, for the first time, investigated in this research. The processing procedure consisted of slurry preparation, tape casting, lamination, binder burn-out, and hot pressing.

Monolithic alumina can be toughened and strengthened by nickel layers in alumina/nickel laminated composites

The strength and apparent toughness of monolithic alumina have been increased to above 700 MPa and 10 MPam$^{1/2}$, respectively, by lamination. The work of fracture in the composites Ni(125), Ni(180), and Ni(240) was 404, 1722, and 2683 J/m$^2$, respectively, as compared to 70 J/m$^2$ for monolithic alumina. It was shown that plastic deformation of ductile lamina, residual compression, and crack renucleation all contribute to toughening in these multilayer composites. No evidence was observed that cracks initiated along the interface or that failure was caused by debonding during flexure fracture. The increment of toughness of the laminates has been found to be proportional to the thickness of the ductile layer. The strength of the laminates was insensitive to flaw size; this fact implies that laminates are

damage tolerant and can be designed using a strength value. The role of residual stresses in the alumina layers was analyzed and discussed. However, a more precise method to characterize the residual stress in the laminates is needed.

## Strength and toughness of alumina/nickel laminates can be controlled using interface design.

Fracture experiments on sandwich models of a single nickel layer bonded between two stiff alumina layers gave an insight into how the plastic deformation of constrained nickel layers was influenced by physical change of the interfacial tortuosity. The plastic behavior was correlated to the toughening magnitude of the ductile layers which are strategically located in brittle laminated composites. Consequently, control of the strength of the bond by modifying the interfacial tortuosity results in control of the interfacial debonding length, and eventually causes control of the work of fracture and the strength. The results of the tensile sandwich model was used to design $Al_2O_3/Ni$ laminated composites. Deformation and fracture results of these composites show conformity to the tensile models and revealed that the toughness and the strength of the composites were a function of the interfacial tortuosity. The results found in this thesis should help laminated composite designers to optimize their mechanical behavior.

## The laminated composites are tolerant to the damage caused by thermal shock

The thermal shock behavior of tape cast alumina/nickel laminated composites exhibit some attractive features. The retained strength after thermal shock at a wide range of temperature differences ($\Delta T = 100$ °C to 1200 °C) was increased by more than 120 MPa increment compared to that of monolithic alumina corresponding to each $\Delta T$. Moreover, the critical quenching temperature difference was enhanced more than 100 °C over the monolithic alumina ($\Delta T_c = 250$ °C). The non-catastrophic fracture feature for the laminated composite is more acceptable for industrial applications. This investigation found that the increase in both resistance of thermal crack initiation and crack propagation is attributed to compressive residual stress existing in the alumina layers and crack blunting by the nickel layers. This type of laminated composite shows a way for improvement of thermal shock resistance capacity and damage tolerance of ceramics.

87